We are IntechOpen, the world's leading publisher of Open Access books Built by scientists, for scientists

4,800
Open access books available

122,000
International authors and editors

135M
Downloads

154
Countries delivered to

Our authors are among the

TOP 1%
most cited scientists

12.2%
Contributors from top 500 universities

CLARIVATE ANALYTICS
BOOK CITATION INDEX
INDEXED

WEB OF SCIENCE™

Selection of our books indexed in the Book Citation Index
in Web of Science™ Core Collection (BKCI)

Interested in publishing with us?
Contact book.department@intechopen.com

Numbers displayed above are based on latest data collected.
For more information visit www.intechopen.com

Tissue Modeling and Analyzing for Cranium Brain with Finite Element Method

Xianfang Yue[*], Li Wang, Ruonan Wang,
Yunbo Wang and Feng Zhou
*Mechanical Engineering School,
University of Science and Technology Beijing, Beijing,
China*

1. Introduction

Numerous methods for measuring intracranial pressure (ICP) have been described, and many of them are suitable for different clinical disorders [1-5]. One method for ICP monitoring is through the ventricular system [6,7], which requires stereotaxic techniques and may not be practical for surgical experiments in the brain regions. Ventricular monitoring of ICP is also associated with intracerebral hemorrhage and infection [6]. Another method to monitor ICP is through the subarachnoid space at the cisterna magna, in which catheter placement may be difficult and dangerous due to the anatomy [8,9]. Some studies monitored ICP via epidural [10,12], which has limitations in measuring acute changes in ICP and is inaccurate in some cases when compared with ventricular monitoring [8]. These methods have many disadvantages of invasion, low-accuracy, cross-infection, etc [13,14]. Although many efforts have recently been made to improve the minitraumatic or non-invasive methods [15-19], noninvasive means of measuring ICP do not exist unfortunately in clinic [20,21]. With the significance of raised ICP in the studies of intracranial pathophysiology, espacially in neurosurgical disorders, it would be valuable to have a simple and reliable method to monitor intracranial pressure (ICP) in clinic. Therefore, the minitraumatic or non-invasive, accurate and simple method to measure ICP is an important question of research in neurosurgery. In this study, we propose a new, minitraumatic, simple, and reliable measurable system that can be used to monitor ICP from the exterior surface of skull bone.

The 'Monro [22] – Kellie [23] doctrine' states that an adult cranial compartment is incompressible, and the volume inside the cranium is a fixed volume thus creates a state of volume equilibrium, such that any increase of the volumes of one component (i.e. blood, CSF, or brain tissue) must be compensated by a decrease in the volume of another. If this cannot be achieved then pressure will rise and once the compliance of the intracranial space is exhausted then small changes in volume can lead to potentially lethal increases in ICP. The compensatory mechanism for intracranial space occupation obviously has limits. When the amount of CSF and venous blood that can be extruded from the skull has been

---

[*] Corresponding Author

exhausted, the ICP becomes unstable and waves of pressure develop. As the process of space occupation continues, the ICP can rise to very high levels and the brain can become displaced from its normal position. Dr. Sutherland firstly perceived a subtle palpable movement within the bones of cranium. Dr. Upledger [24] discovered that the inherent rhythmic motion of cranial bones was caused by the fluctuation of CSF. Accordingly, the cranium can move and be deformed as the ICP fluctuates. By pasting strain foils on the exterior surface of skull bone, the skull strains can be measured with the strain gauge. ICP variation can be obtained through the corresponding processing based on the strains. So the ICP can be monitored by measuring the strains of skull bone [25].

2. Mechanical analysis of cranial cavity deformation

2.1 Mechanical analysis of deformation of the skull as a whole

There are two aspects of effects on forces on the objects. One can make objects produce the acceleration, another is make objects deform. In discussing the external force effect, the objects are assumed to be a rigid body not compressed. But in fact, all objects will deform under loading, but different with the degrees. Here, we will mechanically analyze the overall deformation of cranial cavity under the external force.

(1) Two basic assumptions

To simplify the analysis of deformation of human skull, we assume:

1.   Uniformly-continuous materials

The human skull is presumed to be everywhere uniform, and the sclerotin is no gap in bone of cranial cavity.

2.   The isotropy

The human skull is supposed to have the same mechanical properties in all directions. The thickness and curvature of human skull vary here and there. The external and internal boards are all compact bones, in which external board is thicker than internal board but the radian of external board is smaller than that of the internal board. The diploe is the cancellous bone between the external board and the internal board, which consists of the marrow and diploe vein. The parietal bone is the transversely isotropic material [26], namely, it has the mechanical property of rotational symmetry in any axially vertical planes of skull [27]. The tensile and compressive abilities of compact bone are strong. The important mechanical characteristics of cancellous bone are viscoelasticity [28], which is generally considered as the construction of semi-closed honeycomb composed of bone trabecula reticulation. The main composition of cerebral duramater, a thick and tough bilayer membrane, is collagenous fiber11, which is viscoelastic material [29]. And the thickness of duramater is obviously variable with the changing ICP [30]. The mechanical performance of skull is isotropic along tangential direction on the skull surface [31], in which the performance of compact bone in the external board is basically the same as that in the internal board [32], thus both cancellous bone and duramater can be regarded as isotropic materials [33]. And the elastic modulus of fresh duramater is variable with delay time [34]. And there are a number of sutures in the cranial cavity. But while a partial skull is studied on the local deformation, we can regard each partial skull as quasi-homogeneous

and quasi-isotropic. In addition, the sutures of cranial cavity are also the continuous integration with ages.

(2) Two concepts

1.   stress (σ)

Stress is the internal force per unit area. The calculation unit is kg/cm^2 or kg/mm^2.

2.   Transverse deformation coefficient

When the objects are under tension, not only the length is drawn out from l to l_1, but also the width is reduced from b to b_1. This shows that there are the horizontal compressive stresses in the objects. Similarly, while the object is compressed, not only its length shortens but its width increases. It indicates that the horizontal tensile stress distributes in the objects.

The horizontal absolute deformation is noted as $\Delta b = b - b_1$, and the transverse strain is $\varepsilon_0 = \Delta b / b$.

In mechanics of materials, the transverse strain ε_0 is proportional to the longitudinal strain ε of the same material within the scope of the Hooke theorems' application. The ratio of its absolute value $\mu = |\varepsilon_0| / |\varepsilon|$ is a constant. μ is known as the coefficient of lateral deformation, or Poisson ratio. The Poisson ratio of any objects can be detected by the experiment.

While vertically compressed, the objects simultaneously have a horizontal tension. Therefore, when the head attacked in opposite directions force, the entire human skull will take place the longitudinal compression and transverse tension with the same direction of force. Then the longitudinal compressive stress and the horizontal tensile stress will be generated in the scelrotin. Thus, the stress of arbitrary section along radial direction in shell is just equal to the tangential pulling force along direction perpendicular to the normal vertical when ICP is raised.

2.1.1 The finite-element analysis of strains by ignoring the viscoelasticity of cranial cavity

The geometric shape of human skull is irregular and variable with the position, age, gender and individual. So the cranial cavity system is very complex. Moreover, the cranial cavity is a kind of viscoelactic solid with large elastic modulus, and the brain tissue is also a viscoelastic fluid with great bulk modulus. It is now almost impossible to accurately analyze the brain system. Only by some simplification and assumptions, the complex issues can be made. Considering the special structure of cranial cavity composed of skull, duramater, encephalic substance, etc, here we simplify the model of cranial cavity as a regular geometry spheroid of about 200mm external diameter, which is an hollow equal-thickness thin-wall shell.

The craniospinal cavity may be considered as a balloon. For the purpose of our analysis, we adopted the model of hollow sphere. We presented the development and validation of a 3D finite-element model intended to better understand the deformation mechanisms of human skull corresponding to the ICP change. The skull is a layered sphere constructed in a

specially designed form with a Tabula externa, Tabula interna, and a porous Diploe sandwiched in between. Based on the established knowledge of cranial cavity importantly composed of skull and dura mater (Fig2.1), a thin-walled structure was simulated by the composite shell elements of the finite-element software [35]. The thickness of skull is 6mm, that of duramater is 0.4mm, that of external compact bone is 2.0mm, that of cancellous bone is 2.8mm, and that of internal compact bone is 1.2mm.
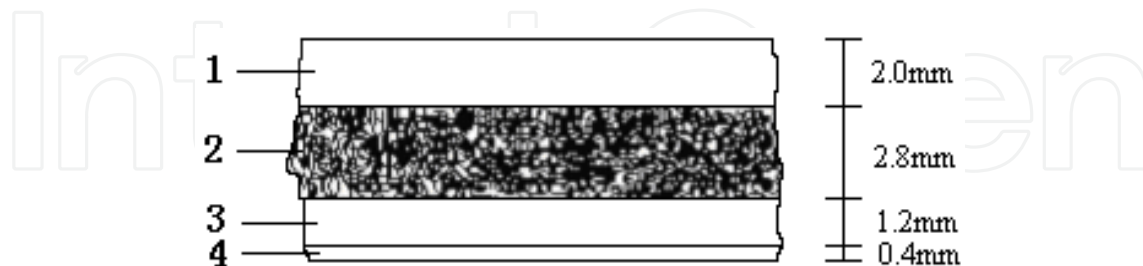

Fig. 2.1. Sketch of layered sphere. The thin-walled structure of cranial cavity is mainly composed of Tabula externa, Diploe, Tabula interna and dura mater.

Above all, we should prove the theoretical feasibility of the strain-electrometric method to monitor ICP. We simplify the theoretical calculation by ignoring the viscoelasticity of cancellous bone and dura mater. And then we make the analysis of the actual deformation of cranial cavity by considering the viscoelasticity of human skull-dura mater system with the finite-element software. At the same time, we can determine how the viscoelasticity of human skull and dura mater influences the strains of human skull respectively by ignoring and considering the viscoelasticity of human skull and dura mater.

2.1.2 The stress and strain analysis of discretized elements of cranial cavity

In order to obtain the numerical solution of the skull strain, the continuous solution region of cranial cavity divided into a finite number of elements, and a group element collection glued on the adjacent node points. Then the large number of cohesive collection can be simulated the overall cranial cavity to carry out the strain analysis in the solving region. Based on the block approximation ideas, a simple interpolation function can approximately express the distribution law of displacement in each element. The node data of the selected field function, the relationship between the nodal force and displacement is established, and the algebraic equations of regarding the nodal displacements as unknowns can be formed, thus the nodal displacement components can be solved. Then the field function in the element collection can be determined by using the interpolation function. If the elements meet the convergence requirements, with the element numbers increase in the solving region with the shrinking element size, and the approximate solution will converge to exact solutions [36].

The solving steps for the strains of cranial cavity with the ICP changes are shown in Fig2.2. The specific numerical solution process is:

1. The discretized cranial cavity

The three-dimensional hollow sphere of cranial cavity is divided into a finite number of elements. By setting the nodes in the element body, an element collection can replace the structure of cranial cavity after the parameters of adjacent elements has a certain continuity.
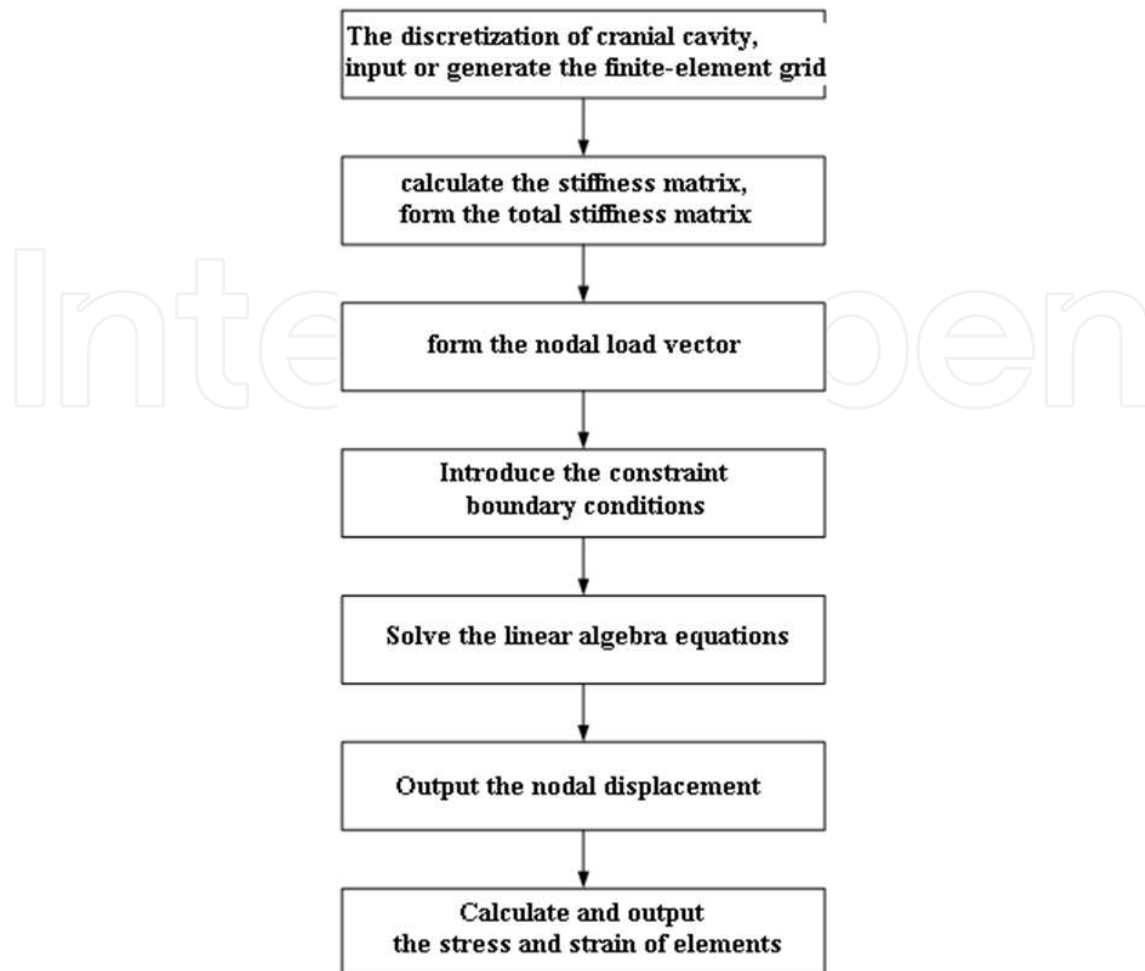
Fig. 2.2. Block diagram of **numerical solution** steps of cranial cavity with the finite-element method

2.   The selection of displacement mode

To make the nodal displacement express the displacement, strain and stress of element body, the displacement distribution in the elements are assumed to be the polynomial interpolation function of coordinates. The items of polynomial number are equal to the freedom degrees number of elements, that is, the number of independent displacement of element node. The orders of polynomial contain the constant term and linear terms.

According to the selected displacement mode, the nodal displacement is derived to express the displacement relationship of any point in the elements. Its matrix form is:

$$\{f\} = [N]\{\delta\}^e \tag{2.1}$$

Where: $\{f\}$ - The displacement array of any point within the element; $[N]$ - The shape function matrix, its elements is a function of location coordinates; $\{\delta\}^e$ - The nodal displacement array of element.

The block approximation is adopted to solve the displacement of cranial cavity in the entire solving region, and an approximate displacement function is selected in an element, where

need only consider the continuity of displacement between elements, not the boundary conditions of displacement. Considering the special material properties of the middle cancellous and duramater, the approximate displacement function can adopt the piecewise function.

3. Analyze the mechanical properties of elements, and derive the element stiffness matrix
a. Using the following strain equations, the relationship of element strain (2.2) is expressed by the nodal displacements derived from the displacement equation (2.1):

Strain equations $\begin{cases} \varepsilon_x = \dfrac{\partial u}{\partial x}, \gamma_{xy} = \dfrac{\partial u}{\partial y} + \dfrac{\partial v}{\partial x} \\[2mm] \varepsilon_y = \dfrac{\partial u}{\partial y}, \gamma_{yz} = \dfrac{\partial u}{\partial z} + \dfrac{\partial w}{\partial y} \\[2mm] \varepsilon_z = \dfrac{\partial u}{\partial z}, \gamma_{zx} = \dfrac{\partial u}{\partial x} + \dfrac{\partial v}{\partial z} \end{cases}$

$$\{\varepsilon\} = [B]\{\delta\}^e \tag{2.2}$$

Where:[B]—The strain matrix of elements; $\{\varepsilon\}$ —The strain array at any points within the elements.

b. The constitutive equation reflecting the physical characteristics of material is $\{\sigma\} = [D]\{\varepsilon\}$, so the stress relationship of stress can be expressed with the nodal displacements derived from the strain formula (2.2):

$$\{\sigma\} = [D][B]\{\delta\}^e \tag{2.3}$$

Where: $\{\sigma\}$ - The stress array of any points in the elements; $[D]$ - The elastic matrix related to the element material.

c. Using the variational principle, the relationship between force and displacement of the element nodes is established:

$$\{F\}^e = [k]^e \{\delta\}^e \tag{2.4}$$

Where: $[k]^e$ - Element stiffness matrix, $[k]^e = \iiint [B]^T [D][B] dx dy dz$; $\{F\}^e$ - Equivalent nodal force array, $\{F\}^e = \{F_V\}^e + \{F_S\}^e + \{F_C\}^e$; $\{F_V\}^e$ - Equivalent nodal force on the nodes transplanted from the element volume force P_V, $\{F_V\}^e = \iiint_V [N]^T \{P_V\} dV$; $\{F_S\}^e$ - Equivalent nodal force on the nodes transplanted from the element surface force, $\{F_A\}^e = \iint_A [N]^T \{P_S\} dA$; $\{F_C\}^e$ - Concentration force of nodes.

4. Collecting all relationship between force and displacement, and establish the relationship between force and displacement of cranial cavity

According to the displacement equal principle of the public nodes in all adjacent elements, the relationship between force and displacement of overall cranial cavity collected from the element stiffness matrix:

$$\{F\} = [K]\{\delta\} \tag{2.5}$$

Where: $\{F\}$- Load array; $[K]$- The overall stiffness matrix; $\{\delta\}$- The nodal displacement array of the entire cranial cavity.

5.   Solve the nodal displacement

After the formula (2.1) ~ (2.5) eliminating the stiffness displacement of geometric boundary conditions, the nodal displacement can be solved from the gathered relationship groups between force and displacement.

6.   By classifying the nodal displacement solved from the formula (2.2) and (2.3), the strain and stress in each element can be calculated.

In this paper, the studied cranial cavity is a hollow three-dimensional sphere, its external radius $R = 100\ mm$, the curvature of hollow shell is $0.01\ \text{rad/mm}$, the thickness of shell wall is 6mm, so the element body of hollow spherical can be treated as the regular hexahedron. The following is the stress and strain analyses in the three-dimensional elements in the cranial space. The 8-node hexahedral element (Fig2.3) is used to be the master element. The origin is set up as the local coordinate system (ξ, η, ζ) in the element. Trough the transformation between rectangular coordinates and local coordinates, the space 8-node isoparametric centroid element can be obtained. The relationship of coordinate transformation is:
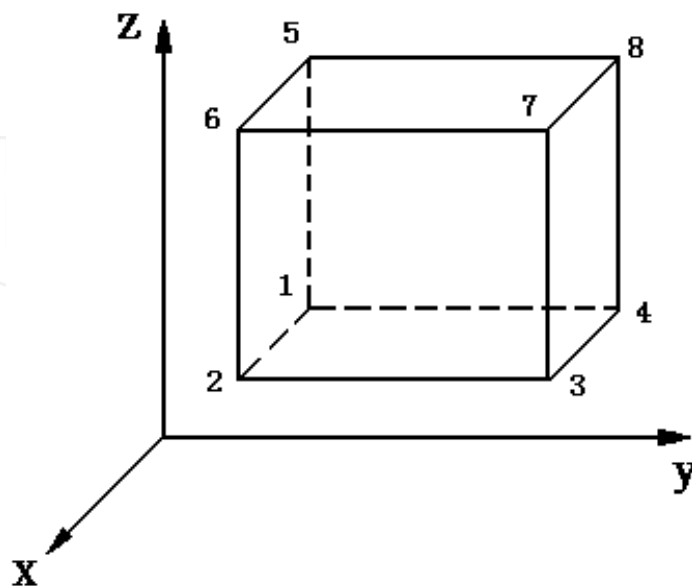

Fig. 2.3. The space 8-node isoparametric centroid element

$$\begin{cases} x = \sum_{i=1}^{8} N_i(\xi,\eta,\zeta)x_i \\ y = \sum_{i=1}^{8} N_i(\xi,\eta,\zeta)y_i \\ z = \sum_{i=1}^{8} N_i(\xi,\eta,\zeta)z_i \end{cases}$$
(2.6)

Then the displacement function of element is:

$$\begin{cases} u = \sum_{i=1}^{8} N_i(\xi,\eta,\zeta)u_i \\ v = \sum_{i=1}^{8} N_i(\xi,\eta,\zeta)v_i \\ w = \sum_{i=1}^{8} N_i(\xi,\eta,\zeta)w_i \end{cases}$$
(2.7)

Where: x_i, y_i, z_i and u_i, v_i, w_i are respectively the coordinate values and actual displacement of nodes.

The element displacement function with matrix is expressed as:

$$\{\delta\} = \begin{Bmatrix} u \\ v \\ w \end{Bmatrix} = \sum_{i=1}^{8} \begin{bmatrix} N_i & 0 & 0 \\ 0 & N_i & 0 \\ 0 & 0 & N_i \end{bmatrix} \begin{Bmatrix} u_i \\ v_i \\ w_i \end{Bmatrix} = \sum_{i=1}^{8} [N_i]\{\delta_i\} = [N]\{\delta\}^e$$
(2.8)

Where: $\{\delta_i\}$ - Nodal displacement array, $\{\delta_i\} = \begin{bmatrix} u_i & v_i & w_i \end{bmatrix}^T$ $(i = 1, 2, \cdots\cdots, 8)$; $\{\delta\}^e$ - The nodal displacement array of entire element, $\{\delta\}^e = \begin{bmatrix} \{\delta_1\} & \{\delta_2\} & \cdots\cdots & \{\delta_8\} \end{bmatrix}^T$; N_i - The uniform shape function of 8 nodes, which can be expressed as:

$$N_i = \frac{1}{8}(1 + \xi_i\xi)(1 + \eta_i\eta)(1 + \zeta_i\zeta) \quad (i = 1, 2, \cdots\cdots, 8)$$
(2.9)

Where: ξ_i, η_i, ζ_i is the coordinates of node i in the local coordinate system (ξ, η, ζ).

The derivative of composite function to local coordinates is:

$$\begin{cases} \dfrac{\partial N_i}{\partial \xi} = \dfrac{1}{8}\xi_1(1 + \eta_1\eta)(1 + \zeta_1\zeta) \\ \dfrac{\partial N_i}{\partial \eta} = \dfrac{1}{8}\eta_1(1 + \xi_1\xi)(1 + \zeta_1\zeta) \\ \dfrac{\partial N_i}{\partial \zeta} = \dfrac{1}{8}\zeta_1(1 + \xi_1\xi)(1 + \eta_1\eta) \end{cases}$$
(2.10)

The strain relationship of space elements is:

$$\{\varepsilon\} = [B]\{\delta\}^e = \sum_{i=1}^{8} [B_i]\{\delta_i\} \tag{2.11}$$

The strain matrix $[B]$ of space element:

$$[B_i] = \begin{bmatrix} \dfrac{\partial N_i}{\partial x} & 0 & 0 \\[2mm] 0 & \dfrac{\partial N_i}{\partial y} & 0 \\[2mm] 0 & 0 & \dfrac{\partial N_i}{\partial z} \\[2mm] \dfrac{\partial N_i}{\partial y} & \dfrac{\partial N_i}{\partial x} & 0 \\[2mm] 0 & \dfrac{\partial N_i}{\partial z} & \dfrac{\partial N_i}{\partial y} \\[2mm] \dfrac{\partial N_i}{\partial z} & 0 & \dfrac{\partial N_i}{\partial x} \end{bmatrix} \tag{2.12}$$

The shape function was derivative to be:

$$\begin{Bmatrix} \dfrac{\partial N_i}{\partial x} \\[2mm] \dfrac{\partial N_i}{\partial y} \\[2mm] \dfrac{\partial N_i}{\partial z} \end{Bmatrix} = [J]^{-1} \begin{Bmatrix} \dfrac{\partial N_i}{\partial \xi} \\[2mm] \dfrac{\partial N_i}{\partial \eta} \\[2mm] \dfrac{\partial N_i}{\partial \zeta} \end{Bmatrix} \tag{2.13}$$

The matrix $[J]$ is the three-dimensional Yake ratio matrix of coordinate transformation:

$$[J] = \begin{Bmatrix} \dfrac{\partial x}{\partial \xi} & \dfrac{\partial y}{\partial \xi} & \dfrac{\partial z}{\partial \xi} \\[2mm] \dfrac{\partial x}{\partial \eta} & \dfrac{\partial y}{\partial \eta} & \dfrac{\partial z}{\partial \eta} \\[2mm] \dfrac{\partial x}{\partial \zeta} & \dfrac{\partial y}{\partial \zeta} & \dfrac{\partial z}{\partial \zeta} \end{Bmatrix} = \begin{bmatrix} \sum\limits_{i=1}^{8} \dfrac{\partial N_i}{\partial \xi} x_i & \sum\limits_{i=1}^{8} \dfrac{\partial N_i}{\partial \xi} y_i & \sum\limits_{i=1}^{8} \dfrac{\partial N_i}{\partial \xi} z_i \\[2mm] \sum\limits_{i=1}^{8} \dfrac{\partial N_i}{\partial \eta} x_i & \sum\limits_{i=1}^{8} \dfrac{\partial N_i}{\partial \eta} y_i & \sum\limits_{i=1}^{8} \dfrac{\partial N_i}{\partial \eta} z_i \\[2mm] \sum\limits_{i=1}^{8} \dfrac{\partial N_i}{\partial \zeta} x_i & \sum\limits_{i=1}^{8} \dfrac{\partial N_i}{\partial \zeta} y_i & \sum\limits_{i=1}^{8} \dfrac{\partial N_i}{\partial \zeta} z_i \end{bmatrix} \tag{2.14}$$

The stress-strain relationship of space elements is:

$$\{\sigma\} = [D]\{\varepsilon\} = [D][B]\{\delta\}^e \tag{2.15}$$

The elasticity matrix $[D]$ is:

$$[D] = \frac{E(1-\mu)}{(1+\mu)(1-2\mu)} \begin{bmatrix} 1 & 0 & 0 & 0 & 0 & 0 \\ \dfrac{\mu}{1-\mu} & 1 & 0 & 0 & 0 & 0 \\ \dfrac{\mu}{1-\mu} & \dfrac{\mu}{1-\mu} & 1 & 0 & 0 & 0 \\ 0 & 0 & 0 & \dfrac{1-2\mu}{2(1-\mu)} & \dfrac{\mu}{1-\mu} & \dfrac{\mu}{1-\mu} \\ 0 & 0 & 0 & 0 & \dfrac{1-2\mu}{2(1-\mu)} & \dfrac{\mu}{1-\mu} \\ 0 & 0 & 0 & 0 & 0 & \dfrac{1-2\mu}{2(1-\mu)} \end{bmatrix} \qquad (2.16)$$

The element stiffness matrix from the principle of virtual work is:

$$[k]^e = \iiint_V [B]^T [D][B] \mathrm{d}x\mathrm{d}y\mathrm{d}z = \begin{bmatrix} k_{11} & k_{12} & \cdots & k_{18} \\ k_{21} & k_{22} & \cdots & k_{28} \\ & \cdots & \cdots & \\ k_{81} & k_{82} & \cdots & k_{88} \end{bmatrix} \qquad (2.17)$$

Where:

$$\left[k_{ij} \right] = \iiint_V [B]^T [D][B] \mathrm{d}x\mathrm{d}y\mathrm{d}z = \int_{-1}^{1}\int_{-1}^{1}\int_{-1}^{1} [B]^T [D][B] J \mathrm{d}\xi \mathrm{d}\eta \mathrm{d}\zeta \qquad (2.18)$$

The equivalent nodal forces acting on the space element nodes are:

$$\{F\}^e = [k]^e \{\delta\}^e \qquad (2.19)$$

Because the internal pressure in the cranial cavity is surface force, the equivalent load for the pressure acting on the element nodes is:

$$\{F_S\}^e = \iint_S [N]^T \{P_S\} \mathrm{d}S \qquad (2.20)$$

The relationship between force and displacement in the entire cranial cavity is:

$$\{F\} = [K]\{\delta\} \qquad (2.21)$$

Then after obtaining the nodal displacement, the stress and strain in each element can be calculated by combining the formula (2.11) and (2.15).

2.2 The stress and strain analysis for complex structure of cranial cavity deformation

Cranial cavity is the hollow sphere formed by the skull and the duramater. From the Fig2.2, there are obvious interfaces among the various parts of outer compact bone, middle

cancellous bone, inner compact bone and duramater, which is consistent with the characteristics of composite materials [37]. Four layered composite structure of cranial cavity is almost lamelleted distribution. Therefore, the lamelleted structure is adopted to establish and analyze the finite-element model of cranial cavity, and the laminated shell element is used to describe the thin cranial cavity made up of skull and duramater. Here the cranial cavity deformation of laminated structure is analyzed as follows:

(1) The stress and strain analysis for the single layer of cranial deformation

Each layers of cranial cavity are all thin flat film. The skulls are transversely isotropic material. The thickness of Tabula externa, diploe, Tabula interna, duramater is all very small. So compared with the components in the surface, the stress components are very small along the normal direction, and can be neglected. So the deformation analysis to single-layer cranial cavity can be simplified to be the stress problems of two-dimensional generalized plane.

The stress-strain relationship of each single-layer structure in the cranial cavity:

$$\{\sigma\} = [Q]\{\varepsilon\} \tag{2.22}$$

Namely:

$$\begin{Bmatrix} \sigma_1 \\ \sigma_2 \\ \tau_{12} \end{Bmatrix} = \begin{bmatrix} Q_{11} & Q_{12} & 0 \\ Q_{21} & Q_{22} & 0 \\ 0 & 0 & Q_{66} \end{bmatrix} \begin{Bmatrix} \varepsilon_1 \\ \varepsilon_2 \\ \mu_{12} \end{Bmatrix} \tag{2.23}$$

Where, 1,2 - The main direction of elasticity in the plane; $[Q]$ - Stiffness matrix,

$Q_{11} = mE_1$, $Q_{12} = m\mu_{12}E_2$, $Q_{22} = mE_2$, $Q_{66} = G_{12}$; $m = \left(1 - \dfrac{\mu_{12}^2 E_2}{E_1}\right)^{-1}$; E_1, E_2 - The elastic

modulus of four independent surfaces in each layer structure; G_{12} - Shear modulus; μ_{12} - Poisson's ratio of transverse strain along the 2 direction that the stress acts on the 1 direction.

(2) The stress and strain analysis for the laminated deformation of cranial cavity

The cranial cavity is as a whole formed by the four-layer structures. So the material, thickness and elastic main direction are all different. The overall performance of cranial cavity is anisotropic, macroscopic non-uniformity along the thickness direction and non-continuity of mechanical properties. Thus, the assumptions need to be made before analyzing the overall deformation of cranial cavity [38]:

1.   The same deformation in each layer

Each single layer is strong glued. There are the same deformation, and no relative displacement;

2.   No change of direct normal

The straight line vertical to the middle surface in each layer before the deformation remains still the same after the deformation, and the length of this line remains unchanged whether before or after deformation;

3. $\sigma_z = 0$

The positive stress along the direction of thickness is small compared to other stress, and can be ignored;

4.   The plane stress state in each single layer

Each single-layer structure is similar to be assumed in plane stress state.

From the four-layer laminated structure composed of Tabula externa, diploe, Tabula interna, duramater, the force of each single-layer structure is indicated in Fig2.4. The middle surface in the laminated structure of cranial cavity is the xy coordinate plane. z axis is perpendicular to the middle surface in the plate. Along the z axis, each layer in turn will be compiled as layer 1, 2, 3, and 4. The corresponding thickness is respectively t_1, t_2, t_3, t_4. As a overall laminated structure, the thickness of cranial cavity is h, shown in Fig2.5.
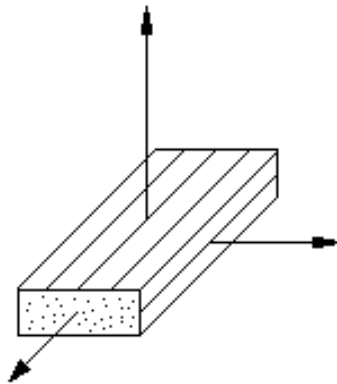
Fig. 2.4. The orientation relationship in each single-layer structure of cranial cavity
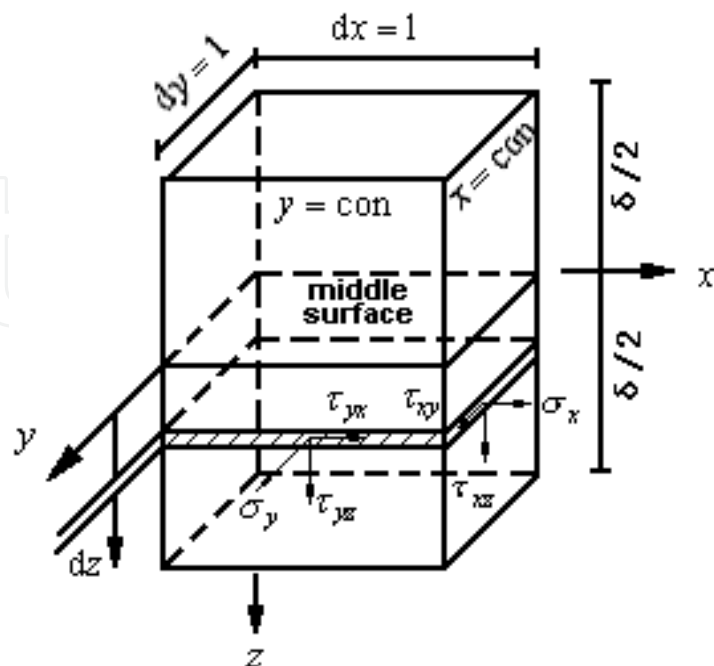
Fig. 2.5. The sketch of four-layered laminated structure of cranial cavity

Then

$$h = \sum_{k=1}^{4} t_k \qquad (2.24)$$

The z coordinates is respectively z_{k-1} and z_k, then $z_0 = -h/2$ and $z_4 = h/2$.

The displacement components at any point within the laminated structure of cranial cavity:

$$\left.\begin{array}{l} u = u(x,y,z) \\ v = v(x,y,z) \\ w = w(x,y,x) \end{array}\right\} \qquad (2.25)$$

The strain is:

$$\left\{\begin{array}{l} \varepsilon_x = \dfrac{\partial u}{\partial x} = \dfrac{\partial u_0}{\partial x} - z\dfrac{\partial^2 w}{\partial x^2} \\[2ex] \varepsilon_y = \dfrac{\partial v}{\partial y} = \dfrac{\partial v_0}{\partial y} - z\dfrac{\partial^2 w}{\partial y^2} \\[2ex] \gamma_{xy} = \dfrac{\partial u}{\partial y} + \dfrac{\partial v}{\partial x} = \dfrac{\partial u_0}{\partial y} + \dfrac{\partial v_0}{\partial x} - 2\dfrac{\partial^2 w}{\partial x \partial y} \end{array}\right. \qquad (2.26)$$

Where: $u = u(x,y,z)$, $v = v(x,y,z)$, $w = w(x,y,z)$ - The displacement components at any point within the cranial cavity; $u_0(x,y)$, $v_0(x,y)$ - The displacement components in the middle surface; $w(x,y)$ - Deflection function, the deflection function of each layer is the same.

Fomular (2.26) can be expressed to be in matrix form:

$$\{\varepsilon\} = \{\varepsilon_0\} + z\{k\} \qquad (2.27)$$

Where: ε_0 - Strain array in the plane, $\{\varepsilon_0\} = \left[\dfrac{\partial u_0}{\partial x}, \dfrac{\partial v_o}{\partial y}, \left(\dfrac{\partial u_0}{\partial y} + \dfrac{\partial v_0}{\partial x}\right)\right]^T$; k - Strain array of

bending in the surface, $\{k\} = \left[-\dfrac{\partial^2 w}{\partial x^2}, -\dfrac{\partial^2 w}{\partial y^2}, -2\dfrac{\partial^2 w}{\partial x \partial y}\right]^T$.

The mean internal force and torque acting on the laminated structure of cranial cavity in the unit width is:

$$\left\{\begin{array}{l} N_i = \displaystyle\int_{-h/2}^{h/2} \sigma_i \mathrm{d}z \\[2ex] M_i = \displaystyle\int_{-h/2}^{h/2} \sigma_i z \mathrm{d}z \end{array}\right. \quad (i = x, y, xy) \qquad (2.28)$$

Taking into account the discontinuous stress caused by the discontinuity along the direction of laminated structure in the cranial cavity, the formula (2.28) can be rewritten in matrix form:

$$\begin{cases} \{N\} = \sum_{k=1}^{n} \int_{z_{k-1}}^{z_k} \{\sigma\} \mathrm{d}z \\ \{M\} = \sum_{k=1}^{n} \int_{z_{k-1}}^{z_k} \{\sigma\} z \mathrm{d}z \end{cases}$$ (2.29)

After substituting the formula (2.22) and (2.27) into equation (2.29), the average internal force and internal moment of the laminated structure in the cranial cavity is:

$$\begin{Bmatrix} N \\ M \end{Bmatrix} = \begin{bmatrix} \sum \int [Q]\mathrm{d}z & \sum \int [Q]z\mathrm{d}z \\ \sum \int [Q]z\mathrm{d}z & \sum \int [Q]z^2\mathrm{d}z \end{bmatrix} \begin{Bmatrix} \varepsilon_0 \\ k \end{Bmatrix} = \begin{bmatrix} A & B \\ B & D \end{bmatrix} \begin{Bmatrix} \varepsilon_0 \\ k \end{Bmatrix}$$ (2.30)

Where: $[A]$ - The stiffness matrix in the plane, $A_{ij} = \sum_{k=1}^{n} Q_{ij}^{(k)}(z_k - z_{k-1})$; $[B]$ - Coupling

stiffness matrix, $B_{ij} = \dfrac{1}{2} \sum_{k=1}^{n} Q_{ij}^{(k)}(z_k^2 - z_{k-1}^2)$; $[D]$- Bending stiffness matrix,

$D_{ij} = \dfrac{1}{3} \sum_{k=1}^{n} Q_{ij}^{(k)}(z_k^3 - z_{k-1}^3)$, $(i, j = 1, 2, 6)$.

Then the flexibility matrix of laminated structure in the cranial cavity is:

$$\begin{bmatrix} a & b \\ c & d \end{bmatrix} = \begin{bmatrix} A & B \\ B & D \end{bmatrix}^{-1}$$ (2.31)

Where: $[a] = [A]^{-1} + [A]^{-1}[B]\left([D] - [B][A]^{-1}[B]\right)^{-1}[B][A]^{-1}$;

$[b] = -[A]^{-1}[B]\left([D] - [B][A]^{-1}[B]\right)^{-1}$; $[c] = -\left([D] - [B][A]^{-1}[B]\right)^{-1}[B][A]^{-1} = [b]^T$;

$[d] = \left([D] - [B][A]^{-1}[B]\right)^{-1}$

Thus, the stress-strain relationship of laminated structure in the cranial cavity is:

$$\begin{Bmatrix} \varepsilon_0 \\ k \end{Bmatrix} = \begin{bmatrix} a & b \\ b^T & d \end{bmatrix} \begin{Bmatrix} N \\ M \end{Bmatrix}$$ (2.32)

With the changing ICP, to determine how the viscoelasticity of human skull and duramater influences the strains of human skull respectively by ignoring and considering the viscoelasticity of human skull and duramater, we make the analysis of the actual deformation of cranial cavity by considering the viscoelasticity of human skull-duramater

system with the finite-element software MSC_PATRAN/NASTRAN and ANSYS. Considering the complexity to calculate the viscoelasticity of human skull and duramater, we can simplify the calculation while on-line analysis only considering the elasticity but ignoring the viscoelasticity of human skull and duramater after obtaining the regularity how the viscoelasticity influences the deformation of cranial cavity.

2.2.1 The finite-element analysis of strains by ignoring the viscoelasticity of human skull and duramater

The craniospinal cavity may be considered as a balloon. For the purpose of our analysis, we adopted the model of hollow sphere (Fig2.6). We presented the development and validation of a 3D finite-element model intended to better understand the deformation mechanisms of human skull corresponding to the ICP change. The skull is a layered sphere constructed in a specially designed form with a Tabula externa, Tabula interna, and a porous Diploe sandwiched in between. Based on the established knowledge of cranial cavity importantly composed of skull and duramater, a thin-walled structure was simulated by the composite shell elements of the finite-element software [39].
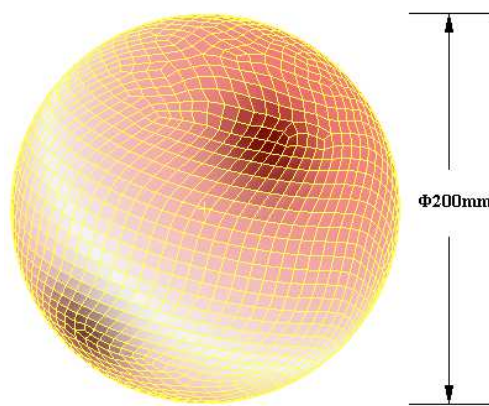
Fig. 2.6. The sketch of 3D cranial cavity and grid division

Of course, the structure, dimension and characteristic parameter of human skull must be given before the calculation. The thickness of calvaria [40] varies with the position, age, gender and individual, so does dura mater [41]. Tabula externa and interna are all compact bones and the thickness of Tabula externa is more than that of Tabula interna. Diploe is the cancellous bone between Tabula externa and Tabula interna [42]. The parietal bone is the transversely isotropic material, namely it has the mechanical property of rotational symmetry in the axially vertical planes of skull [43]. The important mechanical characteristic of cancellous bone is viscoelasticity, which is generally considered as the semi-closed honeycomb structure composed of bone trabecula reticulation. The main composition of cerebral dura mater, a thick and tough bilayer membrane, is the collagenous fiber which has the characteristic of linear viscoelasticity [44]. And the thickness of dura mater obviously varies with the changing ICP [45]. The mechanical performance of skull is isotropic along the tangential direction on the surface of skull bone [46], in which the performance of compact bone in the Tabula externa is basically the same as that in the Tabula interna [47]. Thus both cancellous bone and dura mater can be regarded as isotropic materials. And the elastic modulus of fresh dura mater varies with the delay time [48].

Next we need determine the fluctuant scope of human ICP. ICP is not a static state, but one that influenced by several factors. It can rise sharply with coughing and sneezing, up to 50 or 60mmHg to settle down to normal values in a short time. It also varies according to the activity the person is involved with. For these reasons single measurement of ICP is not a true representation. ICP needs to be measured over a period. Measured by means of a lumbar puncture, the normal ICP in adults is 8 mmHg to 18 mmHg. But so far there are almost no records of the actual human being's ICP in clinic. The geometry and structure of monkey's skull, mandible and cervical muscle are closer to those of human beings than other animals'. So the ICP of monkeys [49] can be taken as the reference to that of human beings'. The brain appears to be mild injury when ICP variation is about 2.5 kPa, moderate injury when ICP variation is about 3.5 kPa and severe injury when ICP variation is about or more than 5 kPa. Therefore, we carried out the following theoretical analysis with the ICP scope from 1.5 kPa to 5 kPa.

In this paper, the finite-element software MSC_PATRAN/NASTRAN and ANSYS are applied to theoretically analyze the deformation of human skull with the changing ICP. The external diameter of cranial cavity is about 200 mm. The thickness of shell is the mean thickness of calvarias. The average thickness of adult's calvaria is 6.0 mm, that of Tabula externa is 2.0 mm, diploe is 2.8 mm, Tabula interna is 1.2 mm and, dura mater in the parietal position is 0.4 mm.

Considering the characteristic of compact bone, cancellous bone and dura mater, we adopt their elastic modulus and Poisson ratios as 1.5×10^4 MPa, 4.5×10^3 MPa [50], 1.3×10^2 MPa [51] and 0.21, 0.01, 0.23 respectively.
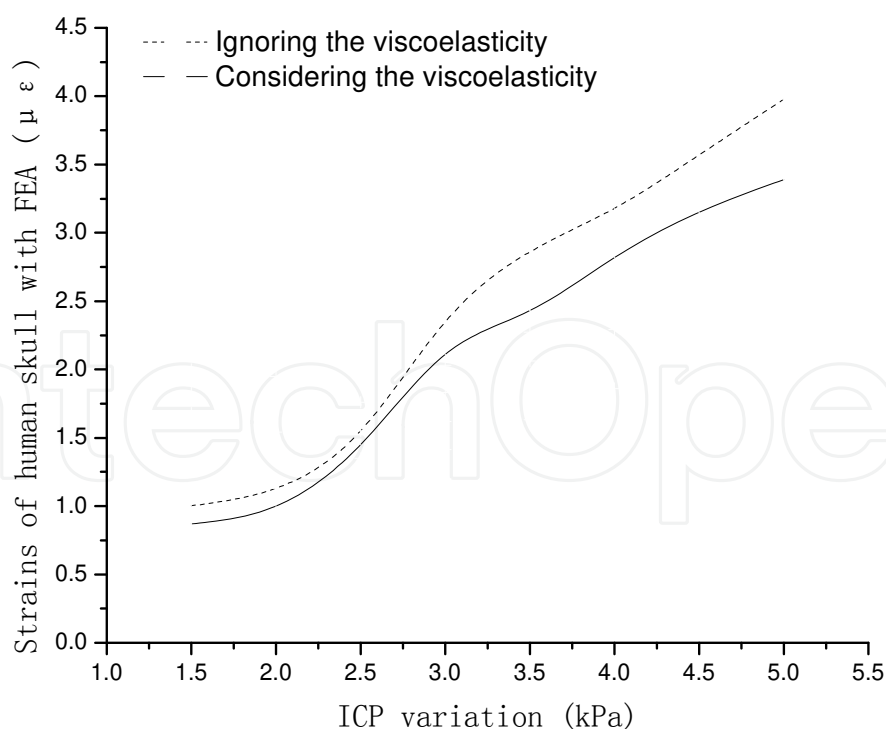
Fig. 2.7. The strain curves of finite-element simulation under the conditions of ignoring and considering the viscoelasticity of human skull and duramater with the changing ICP from 1.5 kPa to 5 kPa

After ignoring the viscoelasticity of human skull and dura mater, the strains of cranial cavity are shown in Table 1 with the finite-element software MSC_PATRAN/NASTRAN as ICP changing from 1.5 kPa to 5.0 kPa (Fig2.7). There is the measurable correspondence between skull strains and ICP variation. The strains of human skull can reflect the ICP change. When ICP variation is raised up to 2.5 kPa, the stress and strain graphs of skull bone are shown in Fig2.8~Fig2.13.
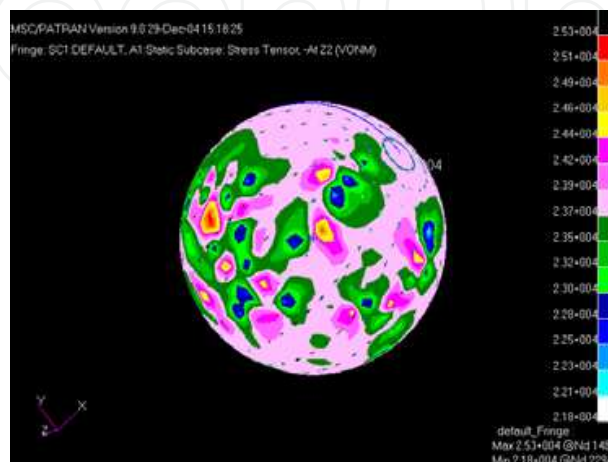

Fig. 2.8. Stress distribution
The scope of stress change on the outside surface is from 22.1 kPa to 25.3 kPa when ICP variation is raised up to 2.5 kPa by ignoring the viscoelasticity of human skull and dura mater.
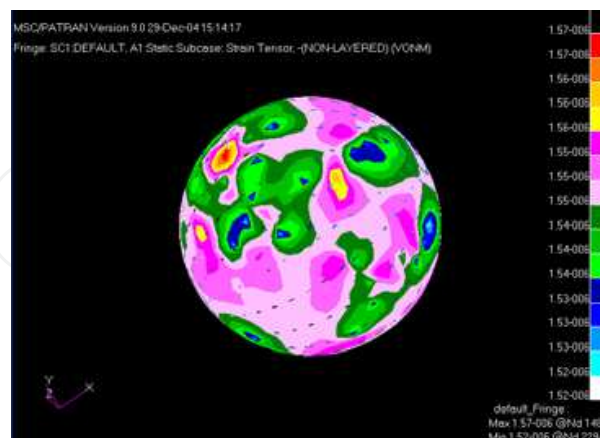
Fig. 2.9. Strain distribution
The scope of strain change on the outside surface is from 1.52 $\mu\varepsilon$ to 1.57 $\mu\varepsilon$ when ICP variation is raised up to 2.5 kPa by ignoring the viscoelasticity of human skull and dura mater.
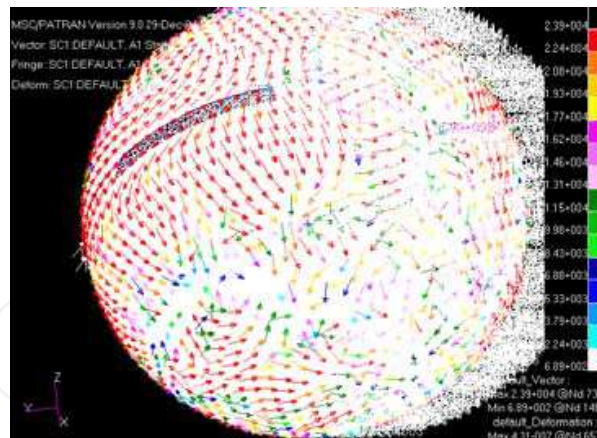
Fig. 2.10. The maximal stress vector distribution
The maximal main stress is about 22.4 kPa when ICP variation is raised up to 2.5 kPa by ignoring the viscoelasticity of human skull and dura mater.
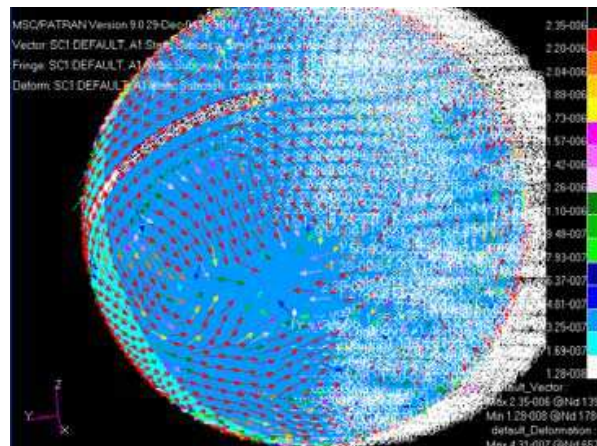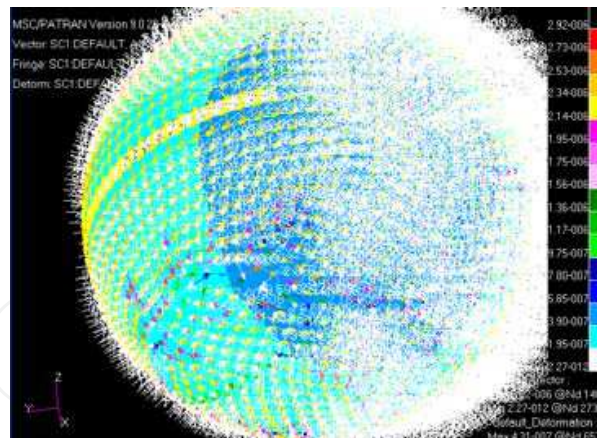

Fig. 2.11. The maximal strain vector distribution
The maximal main strain is about 2.2 $\mu\varepsilon$ when ICP variation is raised up to 2.5 kPa by ignoring the viscoelasticity of human skull and dura mater.
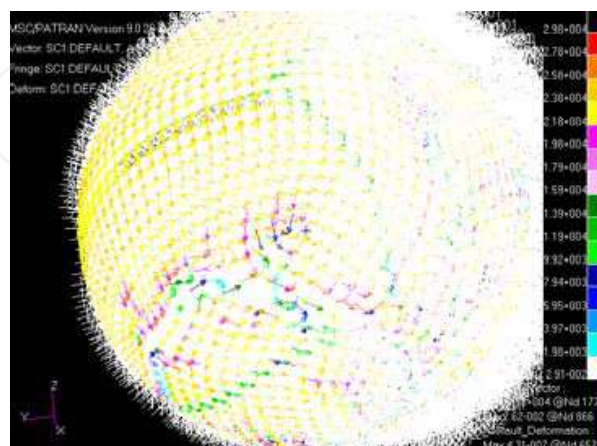
Fig. 2.12. Stress vector distribution
The main stress vector is about 21.8 kPa when ICP variation is raised up to 2.5 kPa by ignoring the viscoelasticity of human skull and dura mater.

Fig. 2.13. Strain vector distribution

The main strain vector is about 2.14 $\mu\varepsilon$ when ICP variation is raised up to 2.5 kPa by ignoring the viscoelasticity of human skull and dura mater.

2.2.2 The finite-element analysis of strains by considering the viscoelasticity of human skull and dura mater

Human skull has the viscoelastic material [52]. Considering the viscoelasticity of human skull and dura mater, we use the viscoelastic option of the ANSYS finite-element program to analysis the strains on the exterior surface of human skull as ICP changing. According to the symmetry of 3D model of human skull, the preprocessor of the ANSYS finite-element program is used to construct a 1/8 finite-element model of human skull and dura mater consisting of 25224 nodes and 24150 three-dimensional 8-node isoparametric solid elements, shown in Fig2.14.
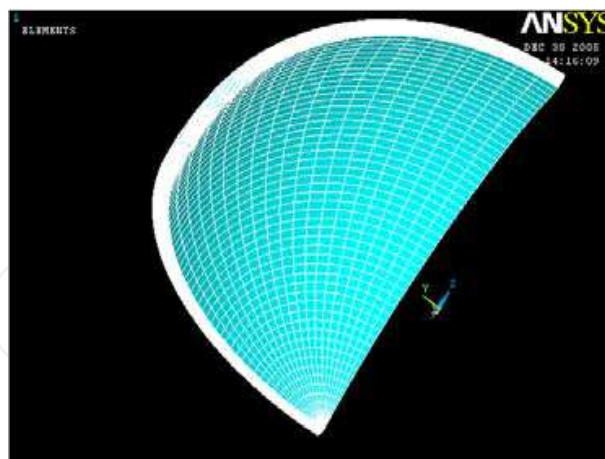
Fig. 2.14. Finite element model of 1/8 cranial cavity shell

The three-dimensional stress-strain relationships for a linear isotropic viscoelastic material are given by:

$$\sigma_{ij} = \int_0^t \left[2G(t-\tau)\frac{\partial e_{ij}(\tau)}{\partial \tau} + \delta_{ij}K(t-\tau)\frac{\partial \theta(\tau)}{\partial \tau} \right] d\tau \; ; \; (i,j=1,2,3) \tag{2.33}$$

Here, σ_{ij} — the Cauchy stress tensor; e_{ij} — the deviatoric strain tensor; δ_{ij} — the Kronecker delta; $G(t)$ — the shear relaxation function; $K(t)$ — the bulk relaxation function; $\theta(t)$ — the volumetric strain; t — the present time; τ — the past time.

Before the theoretical analysis of the minitraumatic strain-electrometric method, we need to set up the viscoelastic models to describe the relevant mechanical properties of human skull and dura mater.

(1) Viscoelastic Model of human skull

Under the constant action of stress, the strain of ideal elastic solid is invariable and that of ideal viscous fluid keeps on growing at the equal ratio with time. However, the strain of actual material increases with time, namely so-called creep. Generally, Maxwell and Kelvin models are the basic models to describe the performance of viscoelastic materials. Maxwell model represents in essence the liquid. Despite the representative of solid, Kelvin model can't describe stress relaxation but only stress creep (Fig2.15). So the combined models made up of the primary elements are usually adopted to describe the viscoelastic performance of actual materials. The creep of linear viscoelastic solid can be simulated by the Kelvin model of three parameters or the generalized Kelvin model.
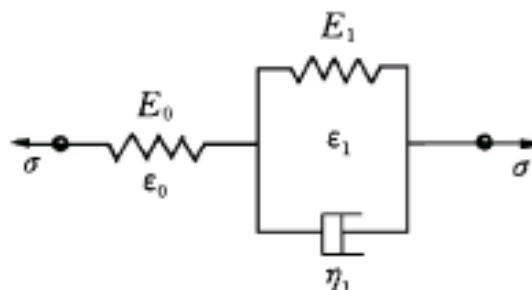
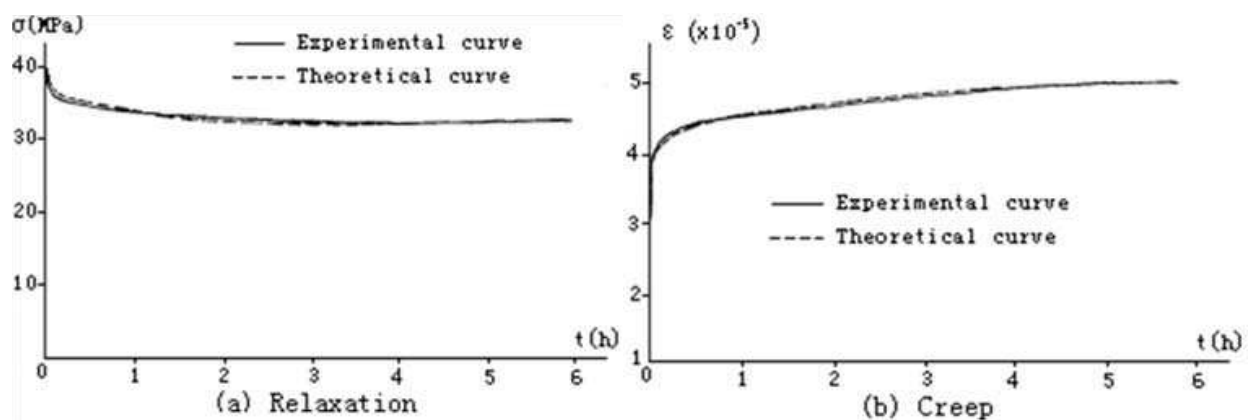Fig. 2.15. Three parameters Kelvin model of human skull.

Fig. 2.16. The relaxation and creep train-time curves between experiment and three parameters Kelvin theoretical model of human skull.

Kelvin model of three parameters is shown in Fig2.15. Fig2.16 (a) is the relaxation curves of human skull and Kelvin model of three parameters in the compressive experiment. Fig2.16(b) is the creep curves of human skull and Kelvin model of three parameters. It shows that the theoretical Kelvin model of three parameters can well simulate the

mechanical properties of human skull in the tensile experiments. Thus the Kelvin model of three parameters is adopted to describe the viscoelasticity of human skull in this paper.

For the Kelvin model of three parameters, the stress and strain of human skull are shown in equation (2.34),

$$\begin{cases} \varepsilon = \varepsilon_0 + \varepsilon_1 \\ \sigma = E_1\varepsilon_1 + \eta\dot{\varepsilon}_1 \\ \sigma = E_0\varepsilon_0 \end{cases} \quad (2.34)$$

After the calculation based on the equation (1), the elastic modulus of human skull is the Fig2.16,

$$E = \left(\frac{E_0E_1}{E_0 + E_1}\right) + \left(\frac{E_0^2}{E_0 + E_1}\right)e^{\frac{t}{P_1}} \quad (2.35)$$

Here, σ — Direct stress acted on elastic spring or impact stress acted on viscopot; ε — Direct strain of elastic spring; E — Elastic modulus of tensile compression; η — Viscosity coefficient of viscopot; $\dot{\varepsilon}$ — strain ratio; $P_1 = \dfrac{\eta}{E_0 + E_1}$.

(2) Viscoelastic Model of human duramater

The generalized Kelvin model is shown in Fig2.17 (c). Fig2.17 (a) is the creep experimental curves of human duramater. Fig2.17 (b) is the curves of creep compliance for the generalized Kelvin model. It shows that the tendency of creep curve in the experiment is coincident with that of creep compliance for the generalized Kelvin model. Creep is the change law of material deformation with time under the invariable stress, so here σ is constant. For the generalized Kelvin model, the stress-strain relationship is $\varepsilon(t) = J(t)\sigma$. Thus the tendency of theoretical creep curve is totally the same as that of experimental one for human duramater. So in this paper, the generalized Kelvin model composed of three Kelvin-unit chains and a spring is adopted to simulate the viscoelasticity of human dura mater in this paper.
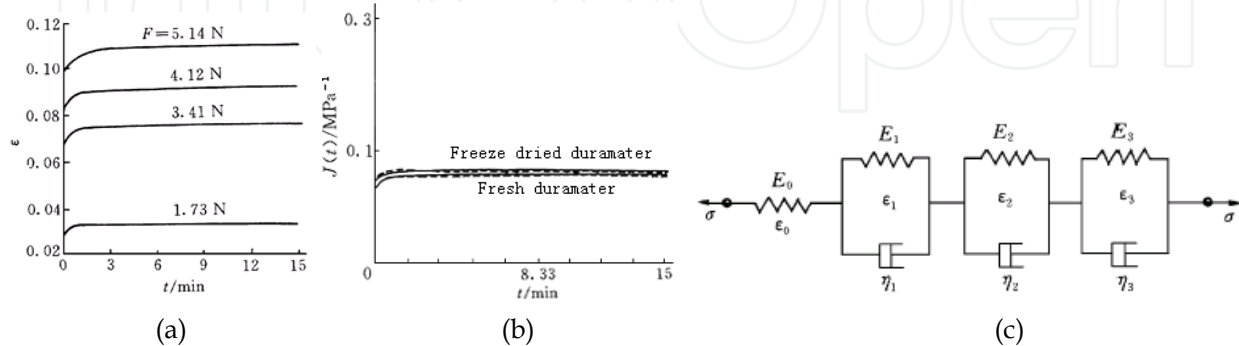

Fig. 2.17. Creep train-time curves under different loads for fresh human duramater (L_0=23 mm, θ=37 °C). Creep compliance curves of human duramatar Kelvin model. And the Kelvin model of the duramater.

For the viscoelastic model of human dura mater composed of the three Kelvin-unit chains and a spring, the stress and strain of human dura mater are shown in equation (2.36),

$$\begin{cases} \varepsilon = \varepsilon_0 + \varepsilon_1 + \varepsilon_2 + \varepsilon_3 \\ \varepsilon_0 = \dfrac{\sigma}{E_0} \\ \sigma = E_1\varepsilon_1 + \eta_1\dot{\varepsilon}_1 = E_2\varepsilon_2 + \eta_2\dot{\varepsilon}_2 = E_3\varepsilon_3 + \eta_3\dot{\varepsilon}_3 \end{cases} \tag{2.36}$$

After the calculation based on the equation (2.36), the creep compliance of human dura mater is equation (2.37),

$$J(t) = E_0^{-1} + E(1 - e^{-t/\tau_1}) + E_2^{-1}(1 - e^{-t/\tau_2}) + E_3^{-1}(1 - e^{-t/\tau_3}) \tag{2.37}$$

Then the elastic modulus of human dura mater is equation (2.38),

$$E = \left[E_0^{-1} + E_1^{-1}\left(1 - e^{-t/\tau_1}\right) + E_2^{-1}\left(1 - e^{-t/\tau_2}\right) + E_3^{-1}\left(1 - e^{-t/\tau_3}\right) \right]^{-1} \tag{2.38}$$

Here, σ, ε, E, η, $\dot{\varepsilon}$ ——Ditto mark; τ_1, τ_2, τ_3 ——Lag time, that is $\tau_1 = \eta_1 / E_1$, $\tau_2 = \eta_2 / E_2$, $\tau_3 = \eta_3 / E_3$.

In the finite-element software ANSYS, there are three kinds of models to describe the viscoelasticity of actual materials, in which the Maxwell model is the general designation for the combined Kelvin and Maxwell models. Considering the mechanical properties of human skull and dura mater, we adopt the finite-element Maxwell model to simulate the viscoelasticity of human skull-dura mater system. The viscoelastic parameters of human skull and dura mater are respectively listed in Table 2.1 and Table 2.2.

	Elastic Modulus (GPa)		Viscosity (GPa/s)	Delay time τ (s)	
	E0	E1	η	τ_γ	* τ_d *
Compression	5.69±0.26	42.24±2.09	26.9±1.5	2022±198	2292±246
Tension	13.64±0.59	51.45±2.54	57.25±4.27	3180±300	4026±372

* $\tau_r = \eta / (E_1 + E_2)$, $\tau_d = \eta / E_2$

Table 2.1. Coefficients for the viscoelastic properties for human skull

	Elastic modulus (MPa)				Delay time τ (s)		
	E_0	E_1	E_2	E_3	τ_1	τ_2	τ_3
Duramater	16.67	125.0	150.0	93.75	40	10^4	10^6

Table 2.2. Creep coefficients for the viscoelastic properties for fresh human duramater

(3) The stress and strain distribution by the finite-element analysis

Fig2.18 (a) ~ (e) are the analytic graphs of stress and strain with finite-element software ANASYS when ICP variation is raised up to 2.5 kPa. After considering the viscoelasticity of human skull and duramater, the stresses and strains of cranial cavity are shown in Fig2.18 as the ICP changing from 1.5 kPa to 5kPa with the finite-element software ANSYS. It shows that the stress and strain distributions on the exterior surface of human skull are well-proportioned and that the stress and strain variation on the exterior surface of cranial cavity is relatively small corresponding to the ICP change. The strains of cranial cavity are coincident with ICP variation. The deformation scope of human skull is theoretically from 0.9 με to 3.4 με as the ICP changing from 1.5 kPa to 5.0 kPa. Corresponding to ICP of 2.5 kPa, 3.5 kPa and 5.0 kPa, the strain of skull deformation separately for mild, moderate and severe head injury is 1.5 με, 2.4 με, and 3.4 με or so.

| Stress nephogram | Strain nephogram | XY shear stress nephogram |

| XZ shear stress nephogram | YZ shear stress nephogram | Interbedded strain change nephogram in the human duramater and skull |
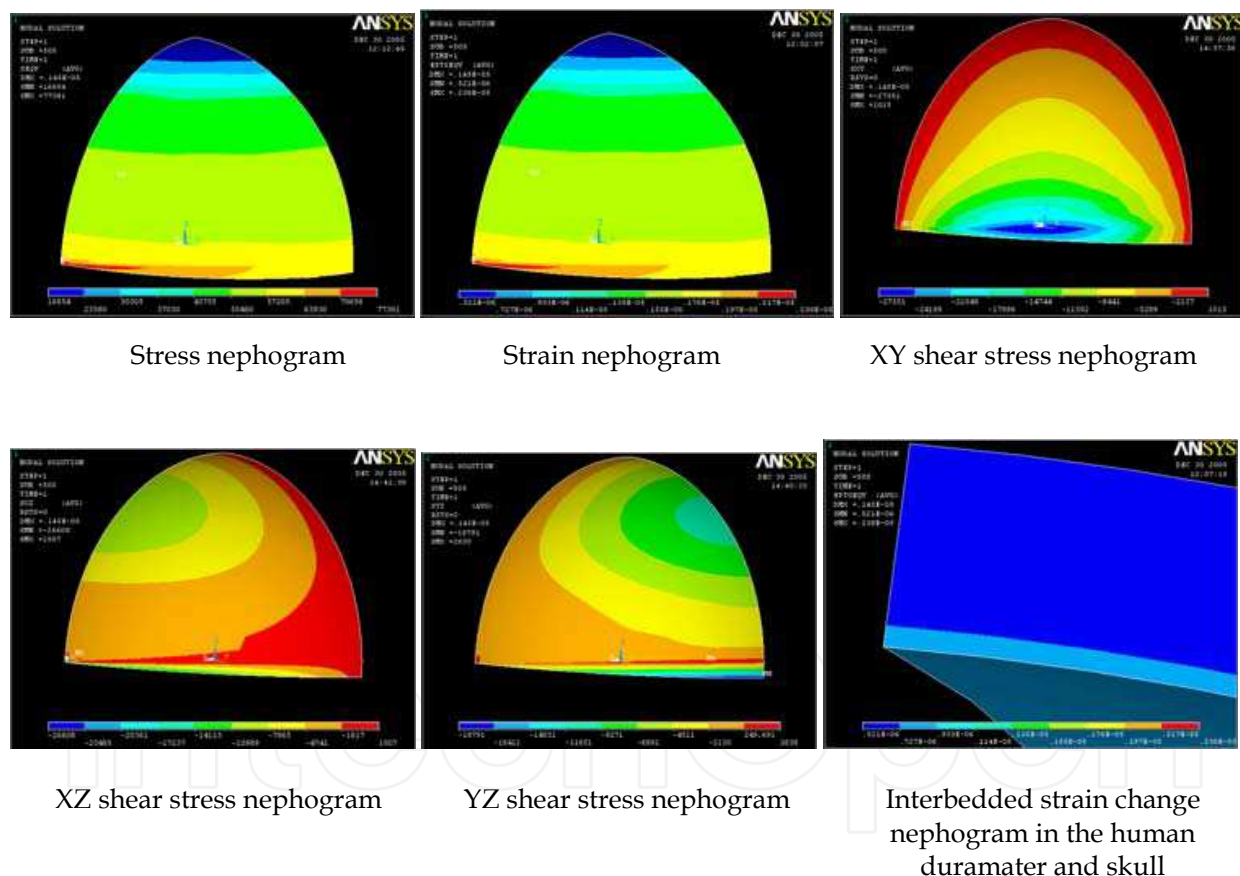
Fig. 2.18. The stress and strain distribution considering viscoelasticity of human skull and duramater

From the relationships about total, elastic and viscous strains of human skull and dura mater in Fig2.19, the viscous strains account for about 40% and the elastic strains are about 60% of total strains with the increasing ICP.
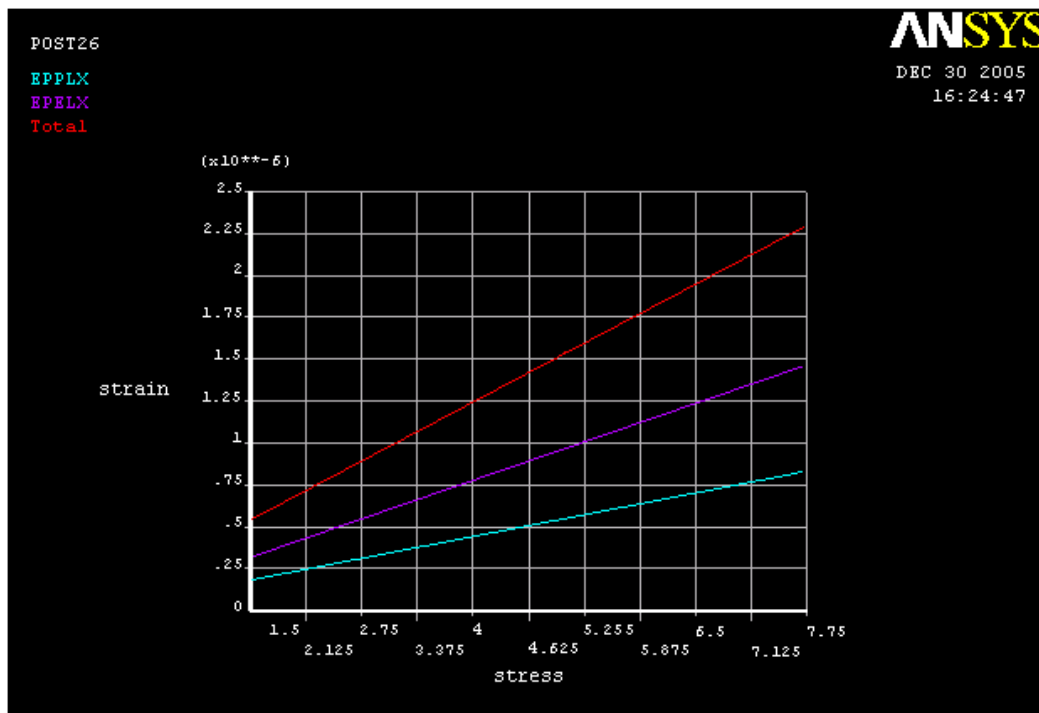
Fig. 2.19. Curves among total, elastic and viscous strain when the ICP increment is 2.5 kPa. Here EPELX is elastic strain curve, EPPLX is viscous strain curve. The viscous strain is about 40% of total strain.

3. Finite-element model of human cranial cavity

3.1 Materials and methods

3.1.1 CT scan

A healthy male volunteer, aged 40 years old, with body height 176 cm, weighing 75 kg, was included in this study. The volunteer explained no history of cranium brain. Common projections (posterior-anterior, lateral, dual oblique, hyperextension and hyperflexion) were made to exclude cranium brain degenerative disorders, cranial instability, and brain destruction.

Spiral CT scans (1 mm thickness) were output in the JPG image file format and saved in the computer. Prior to experiment, informed consent was obtained from this volunteer, shown in Fig3.1.

3.1.2 Experimental equipment

High performance computer (Lenovo, X200) and mobile storage equipment were used. Solid modeling software Mimics 13.0 (Materiaise's interactive medical image control system) was used in this study. As a top software in computer aided design, Mimics 13.0 provides many methods of precise modeling and has been widely used for precise processing. Its equipped Ansys, Partron finite element analysis module sequence were used for finite element analysis, and then the strain and deformation regularity of the real human cranial cavity were simulated with the changing ICP.
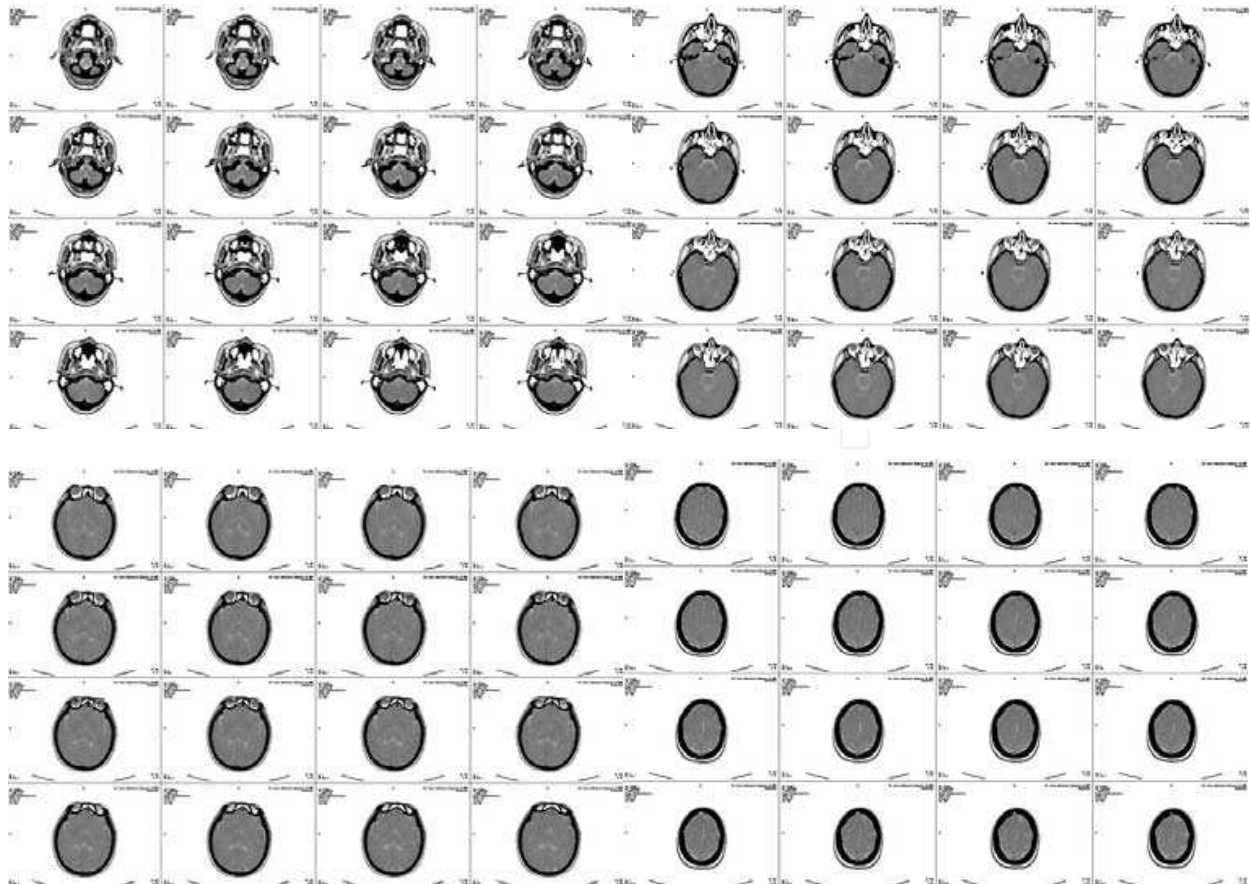
Fig. 3.1. CT scan image of cranial cavity

3.1.3 Flowchart of finite element method

Methods

Image boundary tracking

A self-programmed image boundary automatic recorder was used to acquire cranial information along the superior border to inferior border of cranium brain. The spatial boundary was recorded layer by layer. Following point selection from interior and exterior border of images, two-dimensional space coordinates were automatically recorded and saved in the .CDB form. After conversion, this file can be directly input into Mimics or CAD software.

Location

A coordinate system was determined. The CT scanning image starting from the lowest layer of cranium brain was set as the working background. CT scan was performed based on a fixed coordinate axis, with a know layer interval and magnification proportion. The spatial three-dimensional coordinate of each point in the image could be determined through drawing the horizontal coordinate of each point and referencing scanning interval. When CT machines recorded each layer of images, all images were in the same scanning range, which equaled to cranial location of two-dimensional CT images from each layer in the scanning direction. Calibration of two-dimensional images could be performed if the scar bar of CT scan images

were given. In addition, each layer of image was scanned with some interval in the longitudinal direction, which was equivalent to calibration in the third dimensional direction.

Image reconstruction

In accordance with the sequence of CT scans and according to the scale bar and scan interval of CT faulted image, geometry data of each layer were input into the pre-processing module of finite element software to establish a geometry model in the rectangular coordinate in the sequence of point, line, area, and solid. The transverse plane of CT scan was parallel to xy plane, and the longitudinal plane was along the z axis. Three-dimensional reconstruction process is shown in Fig3.2.
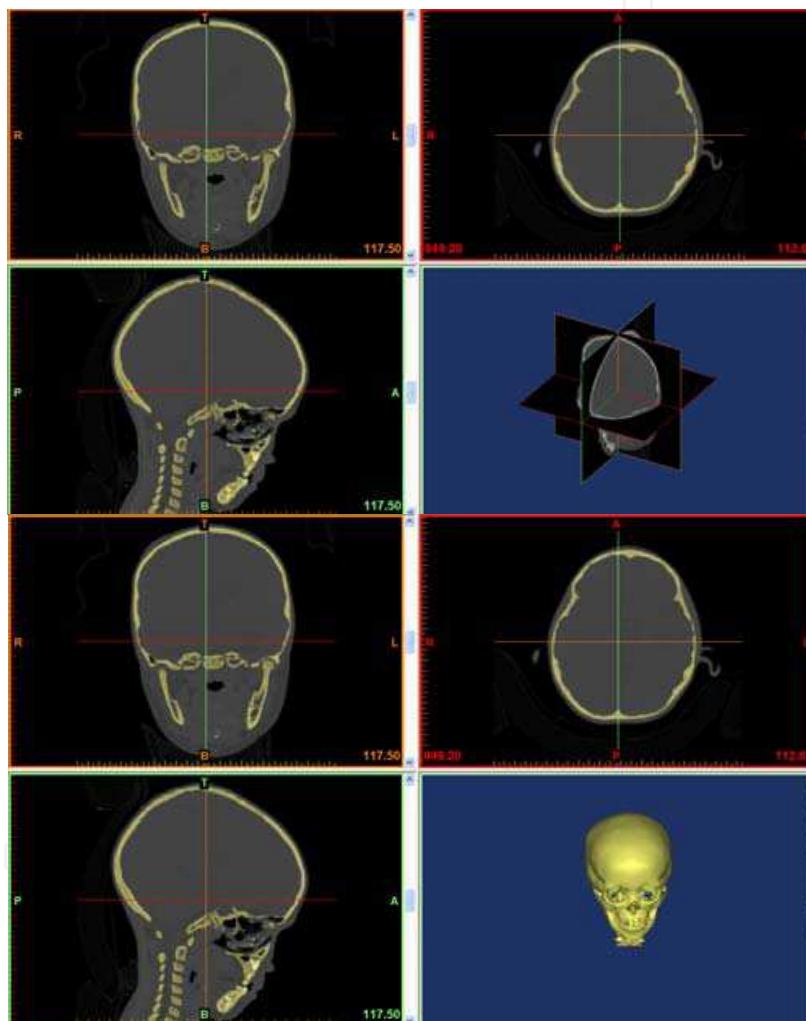
Fig. 3.2. 3d model of cranial cavity

3.2 Results

3.2.1 Reconstruction results

The fitted curves were assigned into different layers to construct the solid structure of bone (Tabula externa, Tabula interna, Diploe sandwiched in between), spongy durameter. During reconstruction of structure of Tabula externa, Tabula interna, Diploe sandwiched in

between, dura mater, solid of each part was generated independently, and the union of all parts was collected. The 3d finite-element models in each direction of cranial cavity are shown in Fig3.3.
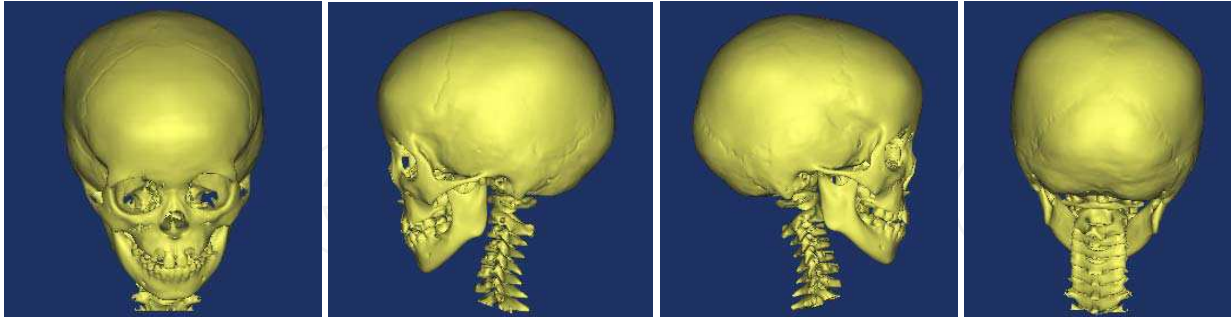
Fig. 3.3. Each view drawing on the 3d finite-element model in of cranial cavity

3.2.2 Model validation

Following type selection, finite element mesh generation was performed in the above-mentioned models which were given material characteristics. Then, through simulating practical situation, boundary condition was exerted and proper numerical process. And the three-dimensional analysis was performed. Based on previously published manuscripts, the elastic modulus and the Poisson's ratio of compact bone, cancellous bone and dura mater, we adopt their elastic modulus and Poisson ratios as 1.5×10^4 MPa, 4.5×10^3 MPa, 1.3×10^2 MPa and 0.21, 0.01, 0.23 respectively. 3d finite-element model of cranial cavity is meshed in Fig3.4. Simulation analysis of cranium brain three-dimensional finite element model is shown in Fig3.5.
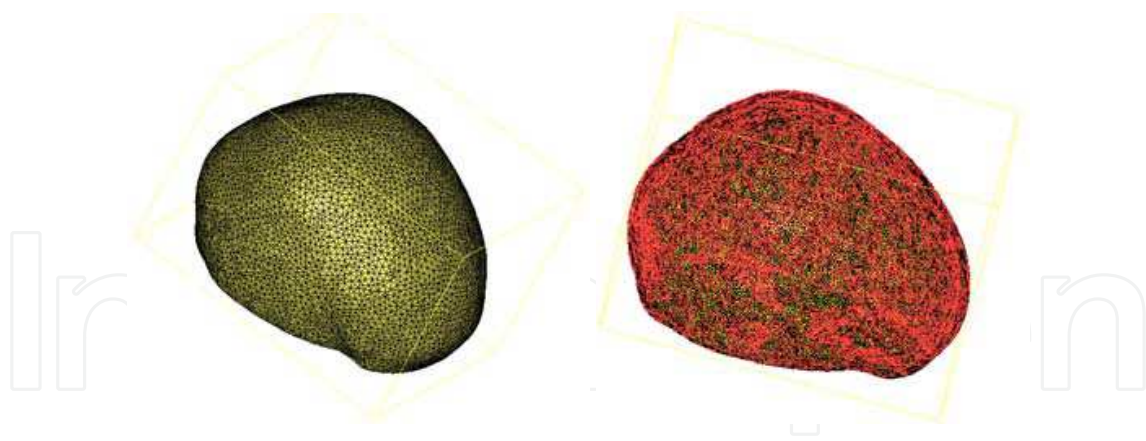
Fig. 3.4. 3d finite-element model of cranial cavity is meshed
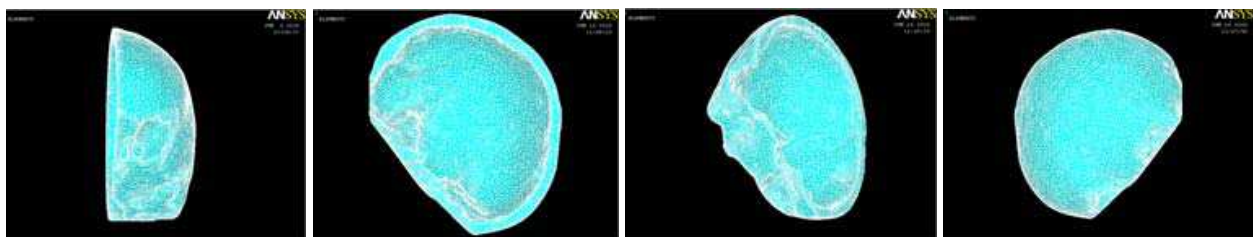
Fig. 3.5. Finite element model of 1/2 cranial cavity

Biomechanical model has been shown to play a key role in study of cranium brain, because it can be used to investigate the pathogenesis through model observation, thereby to propose the strategy of diagnosis and treatment.

Owing to irregular geometry and non-uniform composition of cervical spine cranium bone as well as impossible human mechanical tests, increasing attention has been recently paid to finite element method included in the biological study of cranium brain injury because this method exhibits unique advantages in analysis of complex structure.
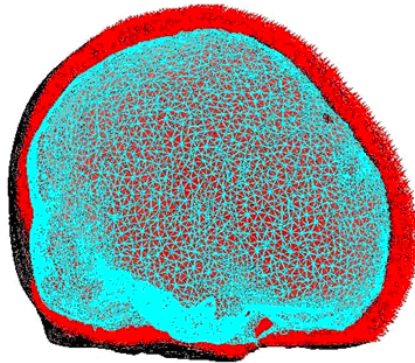
Fig. 3.6. Loads on the finite element model of 1/2 cranial cavity
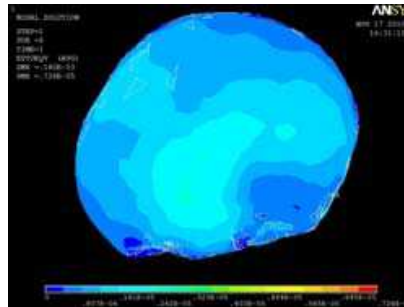
Fig. 3.7. Strain graph when the ICP is 3.0 kPa
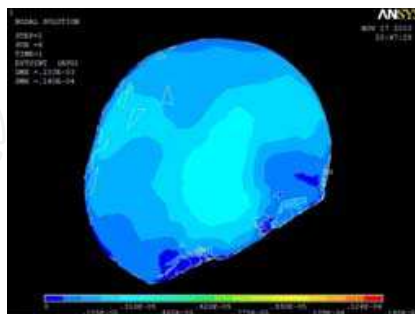
Fig. 3.8. Strain graph when the ICP is 5.0 kPa

Experimental results are the best method to verify model accuracy. When exerting persistent pressure to vertebral spine, non-linear computation is supplemented to the two-dimensional unit calculation of ligament structure, which more corresponds to human mechanical structure. Statics solver exhibits the self-testing function and can automatically analyze computation process, report errors, and control error range. The displacement graph, stress

graph, and isogram drawn by post-processor visualizing the distribution ranges of stress or strain loaded on each part of cranium brain with the changing ICP. When loads are vertically added, the stress on the posterior wall of cranium brain, as well as on the end plate and the posterior part of intervertebral discs, relatively centralizes.
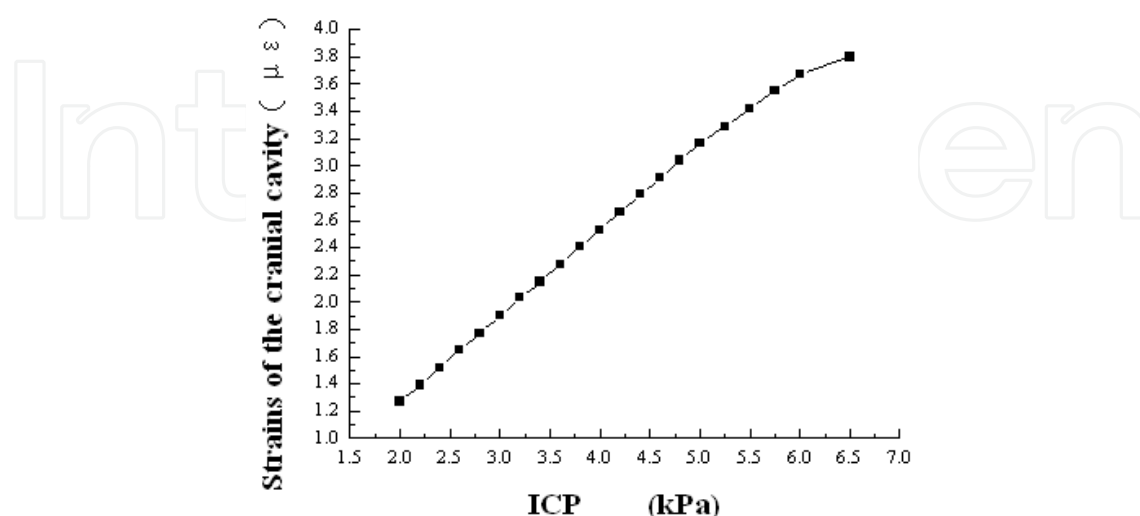

Fig. 3.9. Strains curve of cranial cavity with the ICP variation

3.2.3 Strains on the external surface of cranial cavity

Finite element analysis is an important mean to simulate human structural mechanical function in the field of biomechanics. A human finite element model with physical material characteristics under proper simulated in vivo condition can be used to effectively analyze the physical characteristics of human structure, for example, stress/strain of structure, modal analysis, exterior impact response, and fatigue test. With further understanding of cranium brain diseases, some complex models have not been developed, for example, finite element models of head and cranial cavity used to study the physio-pathological influences cervical spine loading in some complex exercises on cranium brain and soft tissue. Finite element analysis exhibits unexampled advantages in the biomechanical study of a severe medical brain problem. Theoretically, finite element method can simulate nearly all biomechanical experiments. Moreover, this method can better describe the interior changes of living body than practical study. Finite element method, as an emerging technique, has a broad developing space. However, it is a theoretical simulation analyses, only in conjunction with clinical detection and observation can it truly reflect the occurrence and progression of cranium brain disease and provide evidence for predicting curative effects, thereby exhibiting a synergic effect with clinical outcomes. The present model is only a represent. It can not reflect the changes between individual interior parts and between individuals in terms of bone contour and material characteristics. The present model is only a cranium brain motion segment. Its simulation analysis results might differ from the results from multiple motion segments. Actually, when much difference and many uncertainties exist between individuals, model simplification and idealization is to strengthen some research aspect, which removes experimental inherent difference. Of course, establishment of a finite element mechanical model is to provide mechanical methods for clinical and experimental studies. The present model needs further improvements due to some limitations, i.e., unable

to reflect some complex condition, but it ensures the geometry data and material characteristic approximation for application of multiple toolsequipped by various softwares during the process of model establishment. In addition, finite element method, as one of tools used in the biomechanical field, can qualitatively analyze the stress change of cranium brain interior parts when bearing forces. Only by changing local structure or materials can the present model established by finite element method simulate the common clinical situation and the effects of intervention on ICP force. The present model should be further improved in the clinical and experimental processes.

4. Conclusion and discussion

4.1 Conclusion

We develop a new minitraumatic method for measuring ICP with strain-electrometric technology. The strains of skull bone can reflect the ICP change. The surgical procedures for this new method are easy, simple, safe and reliable.

This paper carries respectively on the stress and strain analysis on both conditions of ignoring and considering the viscoelasticity of human skull and duramater by finite-element software MSC_PPATRAN/NASTRAN and ANSYS as ICP changing from 1.5 kPa to 5 kPa. The three-dimensional finite element model of cranial cavity and the viscoelastic models of human skull and duramater are constructed in this paper. At the same time, the ANSYS finite-element software is in this paper used to reconstruct the three-dimensional cranial cavity of human being with the mild hypothermia treatment. The conclusion is as follows:

1. The human skull and duramater are deformed as ICP changing, which is corresponding with mechanical deformation mechanism.
2. When analyzing the strain of human skull and duramater as ICP changing by the finite-element software ANSYS, the strain by considering the viscoelasticity is about 14% less than that by ignoring the viscoelasticity of human skull and duramater. Because the viscoelasticity analysis by finite-element software ANSYS is relatively complex and the operation needs the huge memory and floppy disk space of computer, it is totally feasible to ignore the viscoelasticity while calculating the FEA strain of human skull and duramater as ICP changing.
3. The viscosity plays an important role in the total deformation strain of human skull and duramater as ICP changing. In the strains analysis of human skull and duramater with the changing ICP by the finite-element software ANASYS, the viscous strain accounts for about 40% of total strain, and the elastic strain is about 60% of total strain.
4. Because the strains of human skull are proportional to ICP variation and the caniocerebra characteristic symptoms completely correspond to different deformation strains of human skull, ICP can be completely obtained by measuring the deformation strains of human skull. That is to say, the minitraumatic method of ICP by strain electrometric technique is feasible. Furthermore, ICP variation is respectively about 2.5 kPa when the strain value of human skull is about 1.4 $\mu\varepsilon$, about 3.5 kPa when the strain value of human skull is about 2.1 $\mu\varepsilon$, and about 5 kPa when the strain value of human skull is about 3.9 $\mu\varepsilon$.
5. The strains decreased under the mild hypothermia environment about 0.56% than those under the normal temperature conditions during the same circumstance of ICP changes.

6. The deformation scope of human skull is theoretically from 1.50 $\mu\varepsilon$ to 4.52 $\mu\varepsilon$ as the ICP changing from 2.0 kPa to 6.0 kPa under the normal situation, and from 1.50 $\mu\varepsilon$ to 4.49 $\mu\varepsilon$ under the mild hypothermia environment. Accordingly, the strains of skull deformation for mild, moderate and severe head injuries are separately 1.87 $\mu\varepsilon$, 2.62 $\mu\varepsilon$ and 3.74 $\mu\varepsilon$ or so corresponding to ICP of 2.5 kPa, 3.5 kPa and 5.0 kPa.

4.2 Discussion

In neurosurgery, one of the principle axes of treatment for neurosurgical disease is to control ICP. Because the skull bone is outside of and close to the brain, the surgical procedure in the strain-ICP monitoring system is relatively invasive and may affect experimental results from brain tissue. The strain-ICP monitoring has several advantages. First, the strain foil is far from the brain, and will not affect the surgery or experiments in the brain. Second, the wound surface on the parietal bone is very small and just about 11 mm². Third, the surgical procedure is not extremely invasive for patients compared to the conventional monitoring. Fourth, it is possible to keep the strain foil for a longer time, the fixation of strain foil to the periosteum is much easier than other methods. Fifth, the operation is performed in the cephalic skin, the risk, difficulty, infection and trauma to patients are relatively small. Sixth, no special posture of patients is demanded, skull bone can be hardly influenced by any diseases and will be deformed as long as ICP is fluctuant in brain. ICP can be synchronously and continuously monitored based on the dynamic measurement of skull strains. Thus, this system is relatively safe, and it is easier to keep the strain foils in the cranial cavity for a longer period of time.

In this paper, the finite-element simulation was carried out to analyze the deformation of cranial cavity. Many complex relationships and influencing factors lie in the actual deformation of cranial cavity with the changing ICP. Therefore, in order to obtain the accurate deformation tendency of cranial cavity, the precise simulation to the finite-element model and further experimental studies in vivo and clinic need to be carried on.

5. References

[1] Gregson BA, Banister K, Chambers IR. Statistics and analysis of the Camino ICP monitor. J Neurol Neurosurg Psychiatry 1995; 70: 138.
[2] Hilton G. Cerebral oxygenation in the traumatically brain-injured patient: are ICP and CPP enough? J Neurosci Nurs 2000; 32: 278-282.
[3] Richard KE, Block FR, Weiser RR. First clinical results with a telemetric shunt-integrated ICP-sensor. Neurol Res 1999; 21: 117-120.
[4] Rosner MJ, Becker DP. ICP monitoring: complications and associated factors. Clin Neurosurg 1976; 23: 494-519.
[5] Schmidt B, Klingelhofer J. Clinical applications of a non-invasive ICP monitoring method. Eur J Ultrasound 2002; 16: 37-45.
[6] North B, Reilly P. Comparison among three methods of intracranial pressure recording. Neurosurgery 1986; 18: 730-732.

[7] Powell MP, Crockare HA. Behavior of an extradural pressure monitor in clinical use. Comparison of extradural with intraventricular pressure in patients with acute and chronically raised intracranial pressure. J Neurosurg 1985; 53: 745-749.

[8] Hayes KC, Corey J. Measurement of cerebrospinal fluid pressure in the rat. J Appl Physiol 1970; 28: 872-873.

[9] Melton JE, Nattie EE. Intracranial volume adjustments and cerebrospinal fluid pressure in the osmotically swollen rat brain. Am J Physilo 1984; 246: 533-541.

[10] Andrews BT, Levy M, M cIntosh TK, Pitts LH. An epidural intracranial pressure monitor for experimental use in the rat. Neurol Res 1988; 10: 123-126.

[11] Yamane K, Shima T, Okada Y, Takeda T, Uozumi T. Acute brain swelling in cerebral embolization model of rats. Part I. Epidural pressure monitoring. Surg Neurol 1994; 41: 477-481.

[12] Shah JL. Positive lumbar extradural space pressure. Br J Anaesthesia 1994; 73: 309-314. Sutherland WG. The cranial bowl. Mankato, Minn: Free Press Company 1939.

[13] Zhong J, Dujovny M, Park H, Perez E, et al. Neurological Research 2003; 25: 339-350.

[14] Schmiedek P, Bauhuf C, Horn P, Vajkoczy P, Munch E. International Congress Series 2002; 1247: 605-610.

[15] Allocca JA. Method and apparatus for noninvasive monitoring of intracranial pressure. U.S. Patent 4204547, 1980.3.27.

[16] Rosenfeld JG. Method and apparatus for intracranial pressure estimation. U.S. Patent 4564022, 1986.1.14.

[17] Marchbanks RJ. Method and apparatus for measuring intracranial fluid pressure. U.S. Patent 4841986, 1989.6.27.

[18] Mick EC. Method and apparatus for the measurement of intracranial pressure. U.S. Patent 5074310, 1991.11.24.

[19] Mick EC. Method and apparatus for the measurement of intracranial pressure. U.S. Patent 5117835, 1992.1.2.

[20] Shepard S. Heat trauma. eMedicine 2004; 8: 20.

[21] Czosnyka M, Pickard JD. Monitoring and interpretation of intracranial pressure. J Neurol Neurosurg Psychiatry 2004; 75: 813-821.

[22] Monro A. Observations on the structure and function of the nervous system. Edinburgh, Creech & Johnson 1823; 5.

[23] Kellie G. An account of the appearances observed in the dissection of two of the three individuals presumed to have perished in the storm of the 3rd, and whose bodies were discovered in the vicinity of Leith on the morning of the 4th November 1821 with some reflections on the pathology of the brain. Edinburgh: Trans Med Chir Sci 1824; 1: 84-169.

[24] Retzlaff EW, Jones L, Mitchell Jr FL, Upledger J. Possible autonomic innervation of cranial sutures of primates and other animals. Brain Res 1973; 58: 470-477.

[25] Lakin WD, Stevens SA, Trimmer BI, Penar PL. A whole-body mathematical model for intracranial pressure dynamics. J Math Biol, 2003Apr;46 (4):347-38.

[26] R. M. Jones. Composite Material. 1st Eds. Shanghai Science and Technology Publisher, 1981. 6: 41-73.

[27] Zhimin Zhang. Structural Mechanics of Composite Material. 1st Eds. Beijing: Publish of BUAA, 1993. 9: 85-86.

[28] Willinger, R., Kang, H.S., Diaw, B.M. Development and validation of a human head mechanical model. Comptes Rendus de l'Academie des Sciences Series IIB Mechanics, 1999, 327: 125-131.

[29] Pithioux M, Lasaygues P, Chabrand P. An alternative ultrasonic method for measuring the elastic properties of cortical bone. Journal of Biomechanics 2002; 35: 961-968.

[30] Hakim S, Watkin KL, Elahi MM, Lessard L. A new predictive ultrasound modality of cranial bone thickness. IEEE Ultrason Sympos 1997; 2: 1153-1156.

[31] Hatanaka M. Epidural electrical stimulation of the motor cortex in patients with facial neuralgia. Clinical Neurology and Neurosurgery 1997; 99: 155.

[32] Odgaard A. Three-Dimensional methods for quantification of cancellous bone architecture. Bone 1997; 20: 315-328.

[33] Kabel J., Rietbergenvan B., Dalstra M., Odgaard A., Huiskes R. The role of an elective isotropic tissue modulus in the elastic properties of cancellous bone. Journal of Biomechanics1999; 32: 673-680.

[34] Noort van R., Black M.M., Martin T.R. A study of the uniaxial mechanical properties of human dura mater preserved in glycerol. Biomaterials 1981; 2: 41-45.

[35] Kuchiwaki H., Inao S., Ishii N., Ogura Y., Sakuma N. Changes in dural thickness reflect changes in intracranial pressure in dogs. Neuroscience Letters 1995; 198: 68-70.

[36] Cattaneo P.M., Kofod T., Dalstra M., Melsen B. Using the finite element method to model the biomechanics of the asymmetric mandible before, during and after skeletal correction by distraction osteogenesis. Computer Methods in Biomechanics & Biomedical Engineering 2005; 8(3): 157-165.

[37] Amit G., Nurit G., Qiliang Z., Ramesh R., Margulies S.S. Age-dependent changes in material properties of the brain and braincase of the rat. Journal of Neurotrauma 2003; 20(11): 1163-1177.

[38] Andrus C. Dynamic observation and nursing of ICP. Foreign Medical Sciences (Nursing Foreign Medical Science) 1992; 11(6): 247-249.

[39] Min W. Observation and nursing for fever caused by Acute Cerebrovascular Disease. Contemporary Medicine 2008; 143: 100-101.

[40] Shiozaki T., Sugimoto H., Taneda M., et al. Selection of Severely Head Injured Patients for Mild Hypothermia Therapy. Journal of Neurosurgery 1998; 89: 206−211.

[41] Lingjuan C. Current situation and development trend at home and abroad of Hypothermia Therapy Nursing. Chinese Medicine of Factory and Mine 2005; 18(3): 268-269.

[42] Yue X.F., Wang L., Zhou F. Experimental Study on the strains of skull in rats with the changing Intracranial Pressure.Tianjin Medicine Journal, 2007, 35(2):140-141.

[43] Yue X.F., Wang L., Zhou F. Strain Analysis on the Superficial Surface of Skull as Intracranial Pressure Changing.Journal of University of Science and Technology Beijing, 2006, 28(12):1143-1151.

[44] Qiang X., Jianuo Z. Impact biomechanics researches and finite element simulation for human head and neck.Journal of Clinical Rehabilitative Tissue Engineering Research, 2008, 12(48):9557-9560.

[45] Zong Z., Lee H., Lu C. A three-dimensional human head finite element model and power in human head subject to impact.Journal of Biomechanics, 2006, 39(2):284-292.

[46] Ren L., Hao L., Shuyuan L., et al. A study of the volume of cranial cavity calculating from the dimension of cranial outer surface in X-ray films—its stepw ise regressive equation and evaluation. Acta Anthropological Sinica, 1999, 18(1):17-21.

[47] Yunhong L., Yanbo G., Yunjian W., et al. Experiment study on shock resistance of skull bone. Medical Journal of the Chinese People's Armed Police Forces, 1998, 9(7): 408-409.

[48] Haiyan L., Shijie R., Xiang P., et al. The thickness measurement of alive human skull based on CT image. Journal of Biomedical Engineering, 2007, 24(5):964-968.

[49] Zhou L.F., Song D.L., Ding Z.R. Biomechanical study of human dura and substitutes. Chinese Medical Journal, 2002, 115(11):1657-1659.

[50] Willinger R., Kang H.S., Diaw B.M. Development and validation of a human head mechanical model. Competes Rendus de l'Academie des Sciences Series IIB Mechanics, 1999, 327:125-131.

[51] Odgaard A., Linde F. The Underestimation of young's modulus in compressive testing of cancellous bone specimens. Journal of Biomechanics, 1991, 24, 691-698.

[52] Wenjun S., Jialin H. Handbook of critical illness care. People's Military Medical Press, 1994:75-77.
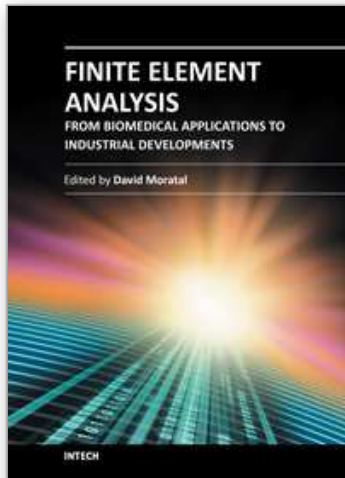
Finite Element Analysis represents a numerical technique for finding approximate solutions to partial differential equations as well as integral equations, permitting the numerical analysis of complex structures based on their material properties. This book presents 20 different chapters in the application of Finite Elements, ranging from Biomedical Engineering to Manufacturing Industry and Industrial Developments. It has been written at a level suitable for use in a graduate course on applications of finite element modelling and analysis (mechanical, civil and biomedical engineering studies, for instance), without excluding its use by researchers or professional engineers interested in the field, seeking to gain a deeper understanding concerning Finite Element Analysis.

INTECH
open science | open minds